ISSN 0255-7193

CLAY RESEARCH

Vol. 33, No. 2

December, 2014

IOS Press

Overseas distribution
IOS Press, The Netherlands

THE CLAY MINERALS SOCIETY OF INDIA
Division of Soil Science and
Agricultural Chemistry
Indian Agricultural Research Institute
New Delhi-110 012, India

Overseas subscribers may send their queries to IOS Press, Nieuwe Hemweg 6B, 1013 BG Amsterdam, The Netherlands, orders@iospress.in: URL: http://www.iospress.nl

THE CLAY MINERALS SOCIETY OF INDIA

(Registered under Act XXI of 1860)
Registration No. S/13028 of 1982

COUNCIL FOR 2014

President	:	Dr. Kunal Ghosh
Vice presidents	:	Dr. Tapas Bhattacharyya
		Dr. Nayan Ahmed
Secretary	:	Dr. Sankar Mahapatra
Joint Secretary	:	Dr. Kaushik Majumdar
		Dr. Gautam Goswami
Treasurer	:	Dr. Jaya N. Surya
Councilors	:	East zone: Dr. Swapna Mukherjee, Dr. R. L. Ram
		West zone: Dr. A.L. Pharande, Dr. Vilas Kharche
		North zone: Dr. H.S. Jassal, Dr. Pankaj Srivastava
		South zone: Dr. S.K. Ghosh Dastidar, Dr. K.S. Anil Kumar
		Central zone : Dr. S.K.Ray, Dr. Tapan Adhikari
Editors, Clay Research	:	Dr. S.C.Datta, Dr. K. M.Manjaiah
Past Presidents	:	Dr. S. K. Mukherjee, Dr. K.V Raman, Dr. S.K. Ghosh, Dr. D.K. Pal, Dr. Dipak Sarkar

EDITORIAL BOARD

International Consulting Editor	:	Dr. S.R. Krishnamurti Gummuluru Adjunct Associate Professor, CERAR, University of South Australia, Canada Dr. Sridhar Komarneni Adjunct Professor of Civil and Environmental Engineering & Editor-in-Chief, J. Porous Materials, USA

Annual Institutional Subscription Rates Inclusive of Air Mail and Handling Charges :

Subscription Rates (Year 2011)	Indian (INR)	Overseas (USD)
Print + online access	Rs. 1,800.00	$ 350.00
Online access	Rs. 600.00	$ 150.00
Print	Rs. 1,200.00	$ 200.00

All payments should be sent to **"The Clay Minerals Society of India"** Division of Soil Science and Agricultural Chemistry, I.A.R.I., New Delhi-110 012

Clay Research, Vol. 33, No. 2, pp. 65-73 (2014)

Characterization of Clays of the Sillon South Rif (Morocco)

LAILA MESRAR AND RAOUF JABRANE

Department of Earth Sciences, Laboratory of Georesources and Environment, Faculty of Science and Technology of Fez, BP.2202, Route d'Imouzzer, Fez (Morocco).

Abstract: *In view of increasing exploitation of clays for the ceramic industry and for the purpose of the value addition of the national natural resource, a study was conducted to characterize the Miocene clay occurring in the Sillon South Rif area of Morocco through geochemical, mineralogical, submicroscopic (scanning electron microscope) and thermogravimetrical analyses. The mineralogical analysis indicated the presence of kaolinite and illite. The geochemical analysis indicated that the major elements of clay samples are mainly composed of silica and alumina alongwith minor amounts of the alkaline oxide and alkaline earth metals. Scanning electron microscopic observations show that the clay matrix is made up of several clay minerals*

Keywords **:** Morocco Clays, Miocene marls, XRD, SEM and Thermal studies,

Clays and clay minerals as very important industrial minerals, used in various application areas such as ceramic, paper, paint, constructions, adsorbent, catalyst are among the most important industrial raw materials (Mesrar, 2012). The suitability of a clay for a specific application is based on its mineralogical and chemical composition. Generally, clays contain different non clay minerals as impurities besides major and minor clay minerals (Mesrar, 2013). Clays containing clay minerals with plate like and fibrous morphology are rare (Harvey, 1996).

These clays are widely used by local people in the diverse needs of pottery and construction, using traditional manufacturing techniques. The importance of clay-based materials in the ceramic industry is resulting from the knowledge of their physical and chemical properties. In this study, we present the characteristics physical, chemical properties of the Miocene clay, which extends over a large area (Fig .1).

A major problem encountered by users of these materials lies in the optimization of the composition of ceramic bodies to improve the yield and quality in manufacturing, enhancement of local

***Corresponding Author Email :** lailamesrar@yahoo.fr.

resources in the region of Fez (Morocco Centre). In view of the present scenario, the present study was aimed at examining natural clay in the region southern Rif groove (Morocco) as no concrete information hitherto not available.

Materials and Methods

Materials

This study was aimed to characterize three marl samples of Miocene age (Fig. 2) which outcrop in the eastern area of Sillon South Rif (Fig. 1) at the quarry. These three samples M1, M2 and M3 are located in the lower, middle and upper stratigraphic series of Miocene marls, respectively (Fig. 2). These samples (M1, M2 and M3) are gray-black in colour. These clays are used for brickyard and pottery in a traditional way.

Because of their plastic properties these clays are used in ceramic industry. However, the complexity of the changes in shape after firing depends on their

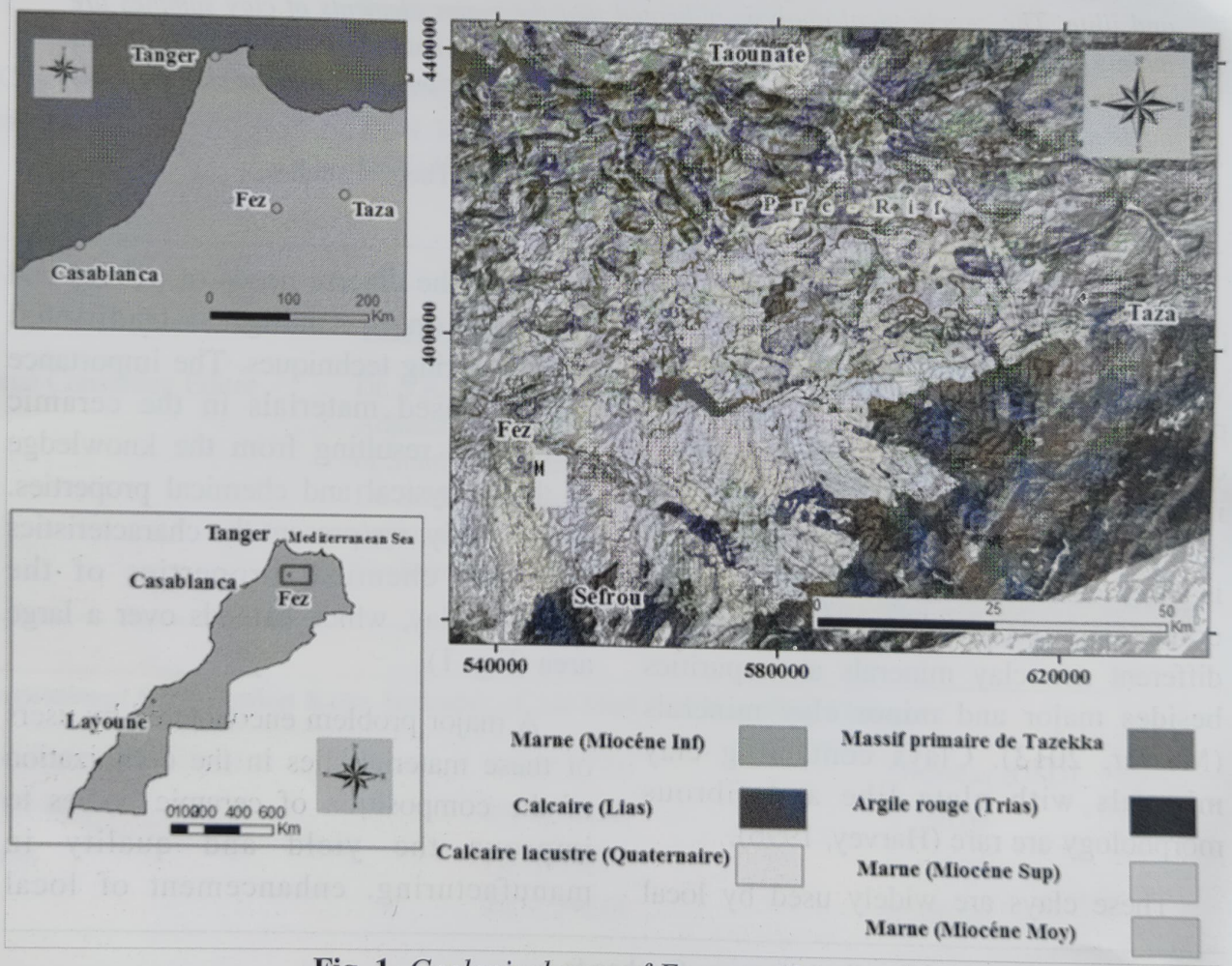

Fig. 1. *Geological map of Fez area (Morocco).*

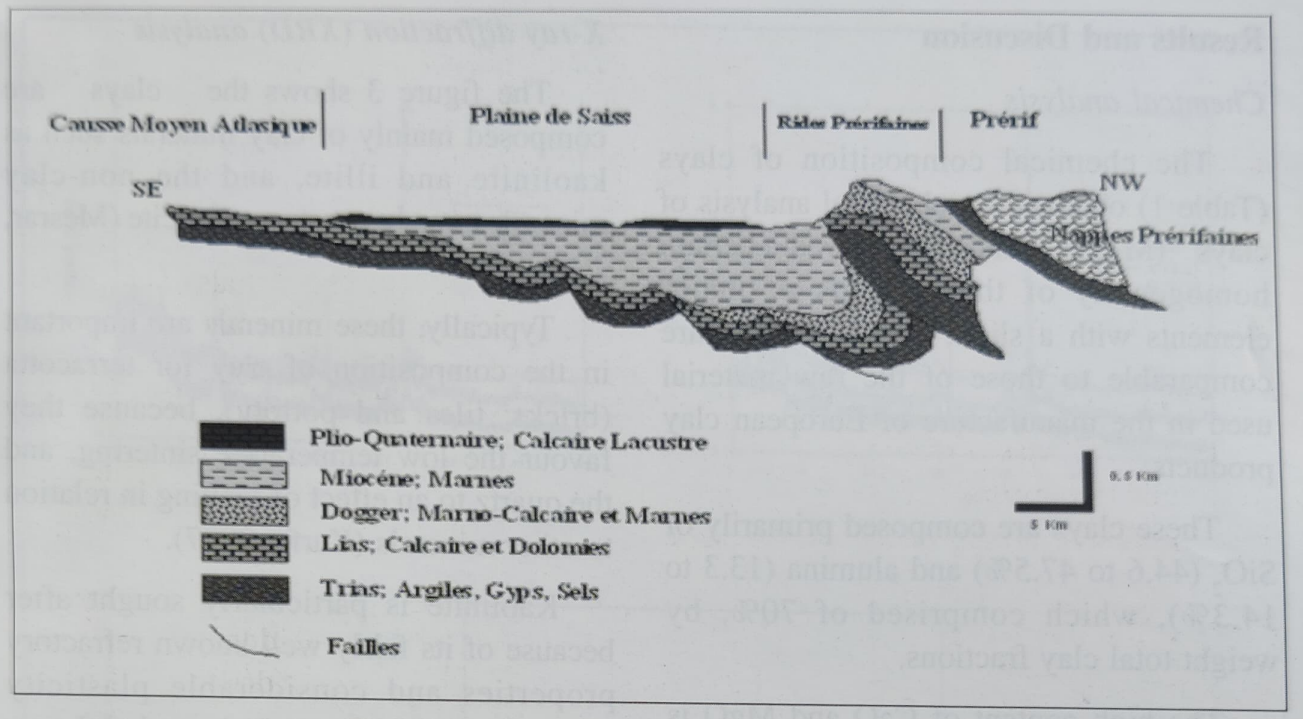

Fig. 2. *Geological cross section of South Rif.*

mineralogical composition and the nature and quantity of impurities. To get a complete knowledge on the characteristic of these clays several analytical techniques were used in the present study.

Chemical analysis

The chemical composition of the clays was determined by X-ray fluorescence spectrometry (Axios, ELE03-PROT ¬v01) using pressed powder pellets.

X ray Diffraction study was carried out in a Philips diffractometer XPERT-PRO" PW 3064, using aNi-filtered Cu Kα radiation operated with 40 kV and 20mA. The diffratograms were obtained from samples treated with ethylene glycol and heated at 550 ° C for 2 h.),

Scanning electron microscope (SEM) examination on the microstructure of the clay samples was observed using SUTW-Sapphire, Resolution: 129.09.

Differential Thermal Analysis (TGA) was performed on all samples at the CNRST, with the appareil type Setaram TGA 24 Setsys series with a temperature ranging from 20 to 950 ° with a heating rate of 10 deg.C min^{-1}.

The mechanical behaviour of briquettes was determined by the elastic limits and breaking effort. The transition from elastic to plastic state is reflected in the appearance of irreversible deformation. This threshold corresponds to the balance limit of a briquette according to the standard (EN 772-1).

Results and Discusion

Chemical analysis

The chemical composition of clays (Table 1) obtained by chemical analysis of clays (M1, M2 and M3) showed a certain homogeneity of the contents of major elements with a slight variation, and are comparable to those of the raw material used in the manufacture of European clay products.

These clays are composed primarily of SiO_2 (44.6 to 47.5%) and alumina (13.3 to 14.3%), which comprised of 70%, by weight total clay fractions.

The high content of CaO and MgO is related to the abundance of carbonate.

Alkalis levels vary between 0.7, 0.8% Na_2O and K_2O between 1 and 1.10%. The samples are relatively rich in iron oxide (5 to 6.20%), which may be due to the presence of either sulphide in the form of free iron oxides such as pyrite. It is likely that the presence of iron responsible for colouring, affecting the color of ceramic tile. In addition, the presence of CaO, MgO, MnO and TiO_2 also affects the colour of the finished product (Mesrar, 2013).

X-ray diffraction (XRD) analysis

The figure 3 shows the clays are composed mainly of clay minerals such as kaolinite and illite, and the non-clay minerals namely quartz and calcite (Mesrar, 2014).

Typically, these minerals are important in the composition of clay for terracotta (bricks, tiles and pottery), because they favour the low temperature sintering, and the quartz to an effect of melting in relation to other minerals (Karfa, 2007).

Kaolinite is particularly sought after because of its fairly well known refractory properties and considerable plasticity (Ferarri, 2006), low drying shrinkage, absence of interlayer swelling and its ability to provide some colourful shards. The mineralogical composition of the clay samples cortege is similar (Fig. 3), which shows a vertical homogeneity of the samples as confirmed by geochemical analysis.

SEM studies

The clay samples under SEM study showed a similarity in microstructure, which is formed by a relatively homoge-

Table 1. *Chemical composition of clay samples (%)*

Nom	SiO_2	Al_2O_3	CaO	Fe_2O_3	MgO	K_2O	Na_2O	TiO_2	P.F%
M1	47.6	13.8	6.90	5.7	2.98	0.95	0.84	0.33	17.3
M2	44.6	14.3	7.28	6.4	3.14	1.02	0.87	0.37	18.6
M3	47	13.3	7.63	6.13	2.71	0.92	0.92	0.31	17.7

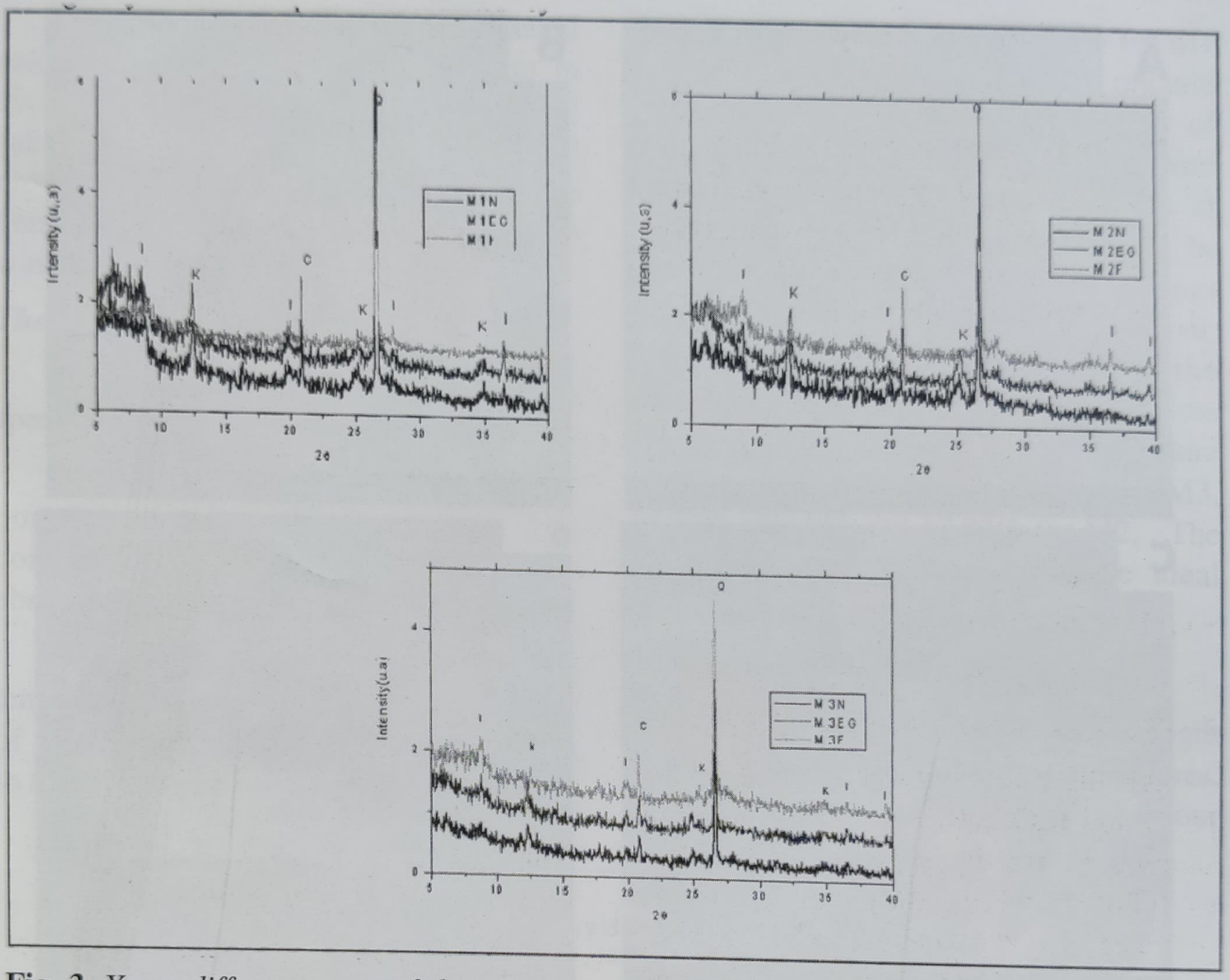

Fig. 3. *X-ray diffractograms of three sample; powdered oriented; EG: treated with ethylene glycol, F: heated at 550 ° C for 2 h, N: Natural. K = kaolinite, Q = quartz, I = illite, C = calcite.*

neous clay matrix (Fig.4.A) and the grains are of variable sizes and tabular form, the pores observed (spaces between clusters and in contact with clay-grain clays) are elongated, their width is generally, less than 5µm (Fig. 4. A), the presence of silica microzone primarily as a structure made of sponge or honeycomb (Fig.4. B), the latter consist of assembling chips apparently linked by silica particles.

Grains of opal are present by their characteristic spherical shape (Fig. 4.E). The opal may prevent alteration of primary components (cristobalite or glass-very siliceous volcanic or biogenic silica) (Mesrar, 2014). The presence of calcite was also noted (Fig.4.C) in significant quantity, which is the result of evaporation of carbonate-rich solution (Claudia, 1999).

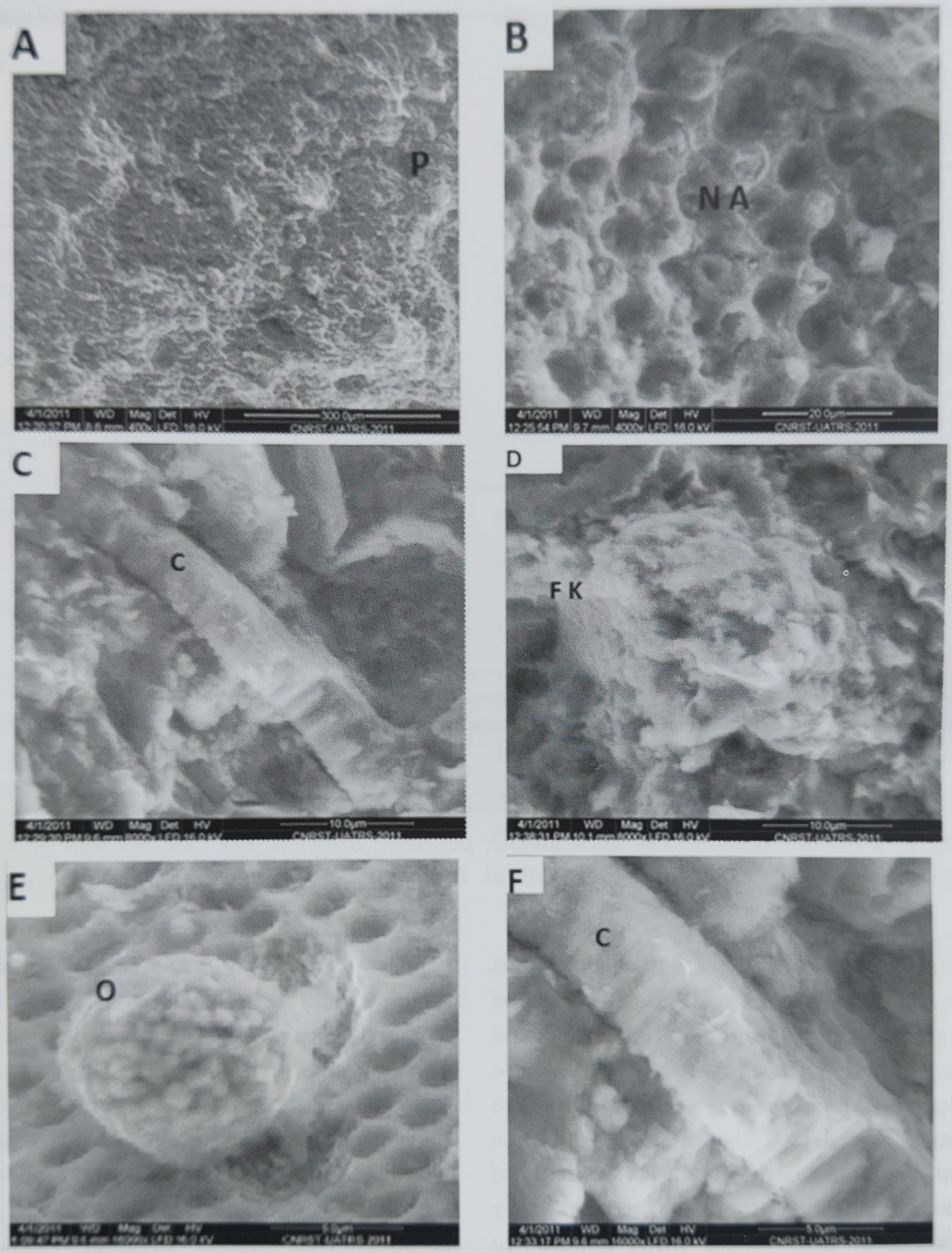

Fig. 4. *The SEM micrograph of clay samples.*

The carbonates consist of an ordered assembly of rods limestone 1 to 2µm in diameter. They are welded by rhombohedral calcite microcrystal that grows in epitaxial growth on calcareous rods (Fig.4.F). The presence of sheets of kaolinite (Fig.4.D) was also noticed.

Thermogravimetric analysis

The thermogravimetric analysis TGA spectra of samples (Fig. 5) shows a

- First-grade between 50°C and 150°C corresponds to a weight loss of 2%, corresponding to the evaporation of water absorbed and zeolitic water (Hellal, 2006).

The second slope appears in the temperature range 350°C and ends at 600°C of significant intensity, which corresponds to a thermal decomposition area with active mass loss of 14% for M2 and 15% for M1 and M3. The decomposition of organic matter to 350°C, and dehydroxylation of the OH groups of silicate layers and hydroxides took place in two stages at 500°C and 640°C. This behaviour can be possibly reported the presence of two types of layer minerals with 1:1 and 2:1 (Baccour, 2011), which is consistent with the mineralogical results. The total mass loss during the heating period, for a temperature not exceeding 800°C, is 16.59% for M3, 17.30% for M1 and 17.83% for M2, . The heating at 800 °C represents the ideal temperature for firing.

Mechanical behaviour

The figure 6 shows the bending strength of clay samples at different temperatures. It was observed that the clay behaviour

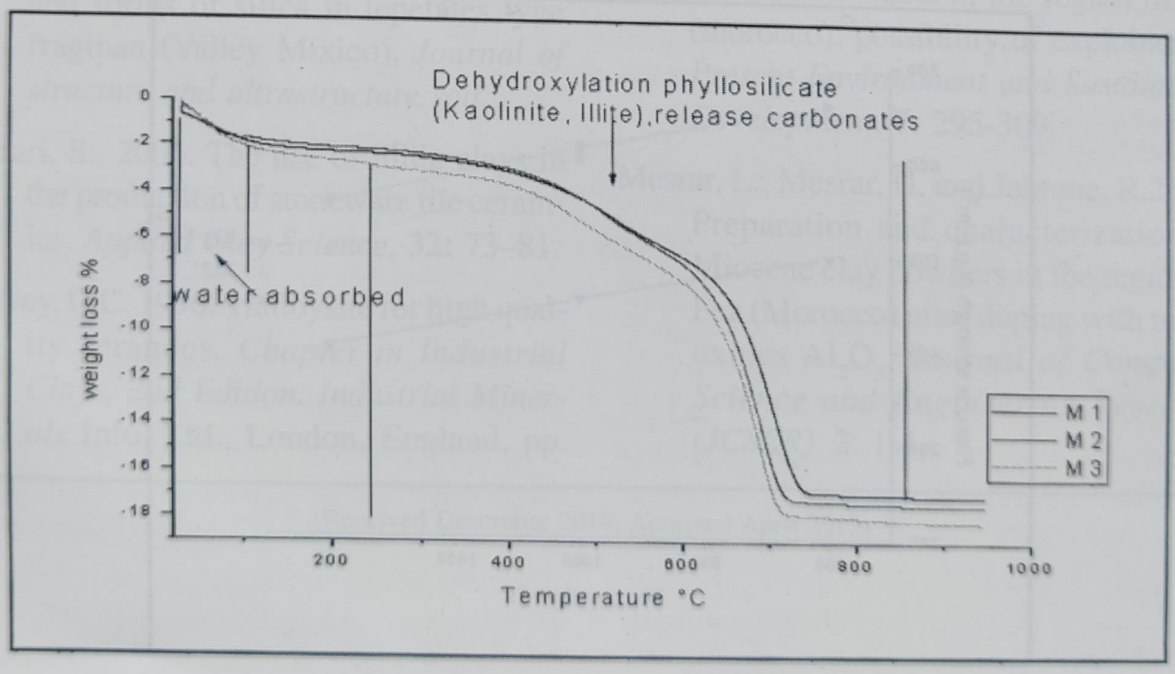

Fig. 5. *Thermogravimetric curve of clay samples.*

remains fragile but greatly improved by cooking.

The explanation for the increase in resistance with temperature up to 900 ° C, is related to the change of crystal structure in the clay material. Indeed, at about 900 °C the cooking destroys all components in clays including organic matter, water, carbonates, oxides, silica, and illite, and that at this temperature the porosity is minimal.

It was noticed that the flexural strength decreased between 1000 ° C and 1100 ° C, and this can be explained by the phenomenon of pocketed structure (Jouenne, 1984). It can be concluded that 900 ° C is the best cooking temperature, or there was a maximum strength.

Conclusions

This study confirms the chemical, mineralogical and mechanical homogeneity in the vertical section of the Miocene clays in the Sillon South Rif, which is consisted of clay minerals such as kaolinite and illite, and the non-clay minerals like quartz and calcite.

Such mineralogical composition of clays broadened their use in ceramic industry (bricks, tiles, floor tiles or wall) and also for the manufacture of ceramic products with high added value such as porcelains.

Acknowledgement

X-ray analysis, FX, SEM, and TGA were carried out at CNRST Rabat.

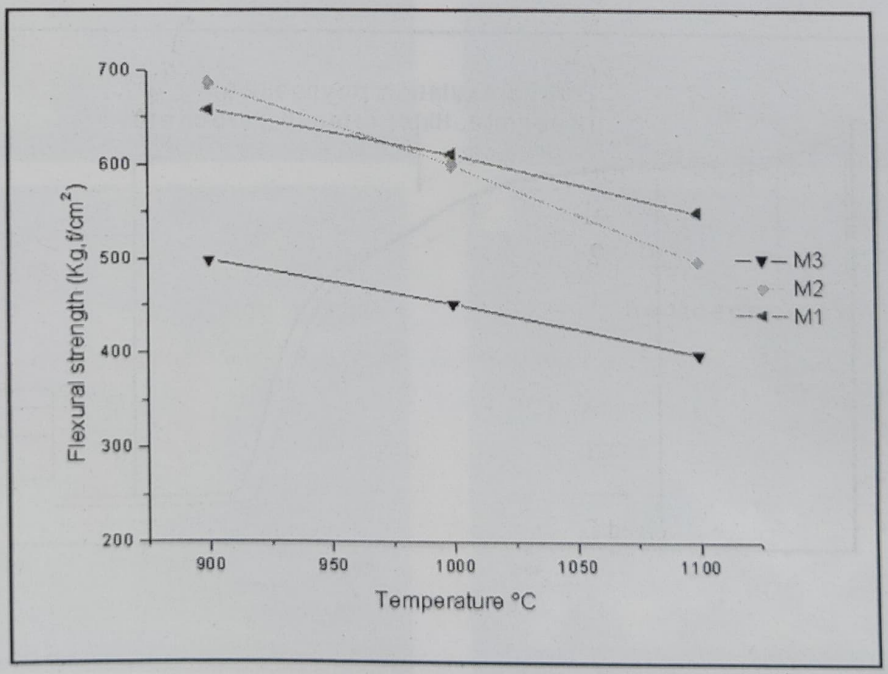

Fig. 6. *The flexural strength of the clays.*

References

Mesrar. L, Akhrif, I. and Jabrane, R. 2014. Technological characterization of the Miocene Marl in the Region of Taza (Morocco), *International Journal of Research in Sciences (IASTER)*, **2**: 8-13.

Mesrar, L., Akhrif, I, and Jabrane, R. 2014 Study of Fe_2O_3 doping effect on the Miocene clays in the region of Taza (Morocco). *Journal of Engineering and Interdisciplinary Research (JEIR)*, **1**: 18-23.

Baccour, Z *et al.*, 2011. Caractérisation physicochimique et mécanique de matériaux céramiques obtenus à partir des argiles tunisiennes, Verres, *Céramiques " Composites,* **1**: 25-33.

Claudia, H., 1999. Nano clays organization and forms of silica in tepetates type fragipan (Valley Mixico), *Journal of structure and ultrastructure soil.*

Ferrari, S., 2006. The use of illitic clays in the production of stoneware tile ceramics. *Applied Clay Science*, **32:** 73–81.

Harvey, C.C. 1996. Halloysite for high quality ceramics. *Chapter in Industrial Clays, 2nd Edition. Industrial Minerals* Info. Ltd., London, England, pp. 71–73.

Hellal, R. 2006. Study and characterization of a kaolinite refractory to tamazert; PhD thesis. *University Physical Science Department,* 119p.

Jouenne, C.A. 1984. Traité de céramiques et de matériaux minéraux. *Ed. Septima, Paris*, 620p.

Karfa, T., 2007. Caractérisation physico-chimique et mécanique de matériaux céramiques obtenus à partir d'une argile kaolinitique du Burkina Faso, *C. R. Chimie* **10** : 511- 517

Mesrar, L. 2012. Characterization of Miocene Marl of Fez Regions of Morocco after doping with MnO_2. *Clay Research,* **31**: 79-83.

Mesrar. L. 2013. Technologycal valorization of Miocene marls in the region of fez (morocco): possibility of exploitation, *Present Environment and Sustainable Development*, **7**: 295-309.

Mesrar, L., Mesrar, H, and Jabrane, R.2014. Preparation and characterization of Miocene clay powders in the region of Fez (Morocco) after doping with metal oxides Al_2O_3. *Journal of Computer Science and Engineering Research (JCSER),* **2**: 1-4.

(Received December 2014; Accepted April 2015)

Clay Research, Vol. 33, No. 2, pp. 74-82 (2014)

KaolinMaze in Clay-Deposits of North-West India

DEEPIKA, KIRAN JEET AND SIDDHARTHA S. MUKHOPADHYAY*

Department of Soil Science, Punjab Agricultural University, Ludhiana 141004, India

Abstract: *Kaolin clays are used as a precursor and raw-material in manufacturing industry. They are abundant in mines spread across the country. They consist of kaolinite and its polymorphs, and halloysite, each species having its characteristics crystallite and charge properties, and surface morphology, and thereby each one of them performs unique tasks. They are in-rerum-natura of novel nanofabrication technology. For example, halloysite might be a substitute of carbon nanotube, especially for farming applications.Similarly,nano-kaolinite and its polymorphs might be useful receptacles for holding anionic plant nutrients. Despite numerous attempts, their precise identification remains inconclusive. We, therefore, attempted to characterize kaolin clays in some of the Indian deposits. They were sampled from five mines of north-west India, and characterized byX-ray diffraction, Fourier Transform Infrared Spectroscopy, and thermal analysis.The simultaneous occurrence of first order X-ray diffraction peaks at 1.01 and 0.93 nm, and absence of 0.7 nm peaks in S1 (Jodhpur), S2 (Delhi), S3 (Udaipur), and S5 (Ahmedabad) samples indicated presence of halloysite. Samples S1 and S2 followed by S4 (Varoda) and S5 showed substantial loss of weight, which could be attributed to the loss of water from their hydration state. Infra-red absorption frequency at 3695, 3676, 3647 and 3620 cm^{-1}in all samples confirmed hydroxyl stretching, but appearance of characteristics bands at 1629 and 1648 cm^{-1} that represent water bending arising from structural and coordinated water in halloysite were observed only in sample S1. Our data confirmed fully hydrated halloysite in sample S1, and partially hydrated halloysite in samples S3 and S4, and samples S2and S5 contain kaolinite or, its polymorphs.*

Key words : Kaolin deposits, North-west India, Characterisation

Since the Neolithic civilization kaolin clays have been used for pottery, and its use as materials spread across various industries since the Industrial Revolution. Clays have been recognized as one of the four prime materials with the advent of nanotechnology (US-EPA, 2007; Johnston, 2010). Kaolin clays occupy a central position in such schemes, and especially perceived to be a wonderful material in nanofabrication and nano-precursor technologies (Mukhopadhyay, 2014). One of its hydrated species, halloysiteis likely to replace carbon nano tube (CNT),

***Corresponding Author Email :** ssmukho@pau.edu; siddharthasm1@gmail.com

especially for farm applications as CNT is toxic to biological systems (Schroeder and Erickson, 2014). In halloysite interlayer water (OH_2) sheet could be stitched together to form nano-tube. Kaolinite; another species in kaolin group that has no interlayer water sheet, on the other hand can be an effective receptacle for retaining anionic plant-nutrient ions like phosphates on octahedral surfaces because of origin of positive charge in octahedral sheet (tetrahedral sheet is negatively charged) (Mukhopadhyay, 2014; Mukhopadhyay and Kalia, 2014a,b). Such distinct structural features, especially crystallite and charge characteristics and interface properties give rise to characteristics bonds that are crucial for nanofabrication (Hall, 2006). The diversity of material properties within kaolin group of clays highlights the necessity of exact characterization.

Attempts have been made to use X-ray diffraction (Dixon, 1989), infrared spectroscopy (Frost *et al.,* 2010), Raman Spectroscopy (Frost, 1995), and use of non-crystallite materials (e.g., amides; Churchman and Theng, 1984) to distinguish species of kaolin group of minerals, but they remained inconclusive (Jousseinet *al.*, 2005). Some of the challenges originate from crystalline properties as halloysite:(i) stays in strongly to weakly hydrated states at 1.0 and 0.7 nm basal spacing, (ii) its interlayer (ab) face is occupied by only 4 molecules of water instead of 6, (iii) its interlayer water-sheet has hydrogen bond within themselves, but weaker bonds between interlayer water-sheet and neighboring alumino silicate sheets, and (iv) water sheet occupies 0.1144 nm^2 on each of aluminosilicate surfaces, but as two surfaces are adjacent to one H_2O, the aluminosilicate surface in contact with H_2O is 0.2290 nm^2 area; twice of its surface (Newman, 1987). Some other challenges come from sample preparation and at instrumental analytical stages as air-drying of sample is essential during which desiccation of halloysite may occur. Similarly because of its structural vulnerability halloysite often gets dehydrated due to generation of heat in the chamber of the instruments (Newman, 1987). India has large reserve of kaolin spread across the country, but it is at the bottom of global utilization of the material. In the absence of precise characterization of the indigenous materials,Indian industries have little options, but to depend on import of kaolin (U.S. Geological Survey Commodity Summary, 2011).

In view of the above scenario, we attempted to use X-ray diffraction in conjunction with thermal and infrared spectroscopy to characterize kaolin clay deposits of north-west India so that they could be utilized for various nanofabrications and other sophisticated industrial manufacturing processes.

Materials and Methods

Naturally occurring kaolin clay samples

were obtained from five firms *viz.* (i) M/s Neelkanth Mineral and Chemical Manufacturers, Jodhpur, (ii) M/s Surya Min Chem, Delhi, (iii) M/s Kamlesh Minerals, Udaipur, (iv) M/s Koat Manufacturing Company, Vadodara, and (v) M/s Futura Ceramics Private Limited, Ahmedabad. The samples were analyzed by X-ray Diffraction techniques (XRD), thermal analysis, and Infrared Spectroscopy (Fourier Transformed IR).

Preparation and purification of homoionic form of kaolin: Kaolin clay was washed repeatedly with distilled water to remove impurities. It was then washed fourtimes with 1N Ammonium Chloride (AR), followed by washing with 90% ethanol till excess $NH_4^+$was removed. The yield wasNH_4^+ saturation (homocationic) on cation exchange sites, and Cl^-saturation (homoanionic) on anion exchange sites. The removal of excessions was confirmed through $AgNO_3$ test.

*X-ray Diffraction:*Magnesium saturated oriented (along the 001 plane) clays were mounted on glass slides and air dried. Copper-Kα X-ray diffraction was obtained at 40 kV voltage with 20 mA current in the Phillips Diffractometer PW1710. The samples were scanned from 2°-30° (2θ) with step size of 0.5° (2θ) at scanning speed of 1° 2θ min^{-1}.

Thermal analysis: Ten gram sample was heated in the temperature range of 80-200° C by 20° C interval steps. At every 20° C increase in temperature, clay was weighed. The thermogravimetric curve was obtained by plotting the weight (w)against temperature (T in ° C).

Fourier Transform Infrared Spectroscopy (FTIR): One mg of air-dry clay was mixed with 100 mg of spectroscopic grade KBr, and ground with mortar and pestle. The mixture was placed into the die set and pressed with the hydraulic pressure for the stroke of at least 10 cm that created pressure at 125 kg cm^{-1} on the confined sample. This yielded about 1 mm thick and 13 mm diameter pellets.Then the pellets were placed in the sample holder and samples were analyzed in the frequency range of 400-4000 cm^{-1} using Thermo Nicolet 6700 Fourier Transform Infrared Spectrometer.

Results and Discussion

X-ray Diffraction: The X-ray diffraction obtained from basally oriented samples occurred at 2θ=8.8°, which corresponds to d-spacing of 1.0119 nm (Fig. 1). The simultaneous occurrence of distinct first order peaks at 1.01 and 0.93 nm, and absence of 0.7 nm peaks confirmed the presence of halloysite in S1, S2, S3, and S5 samples (Table 1). They were also indicative of state of moderate hydration in halloysite. The1.01 nm peak is broader towards lower angle and weaker than the neighbouring 0.93 nm peak, alongside blurring of 002 and 003 basal reflections, which are reflective of structural disorder in halloysite. Such disorder due to displacement of octahedral vacant site was

also reported by Dixon (1989). In S1, S2, and S3 samples, the XRD basal reflections (Fig.1) show strong sharp peaks at 0.93, 0.46 and 0.33 nm, indicating that the samples also contained illite (fine-grained mica). Occurrence of illite along with halloysite had been reported from Georgia earlier (Lee *et al.,* 1975). In the S4 sample, occurrence of high intensity sharp peaks at 0.71 and 0.35 nm confirmed the presence of kaolinite.Although the exact reason of structural disorder in halloysite is difficult to discern, it could be perceived to be due to prolonged lattice stress.

Thermal analysis : Sample S1 lost weight all through the temperature range of 80-200° C (Fig. 2). It indicates that the material was free from transition elements like Fe

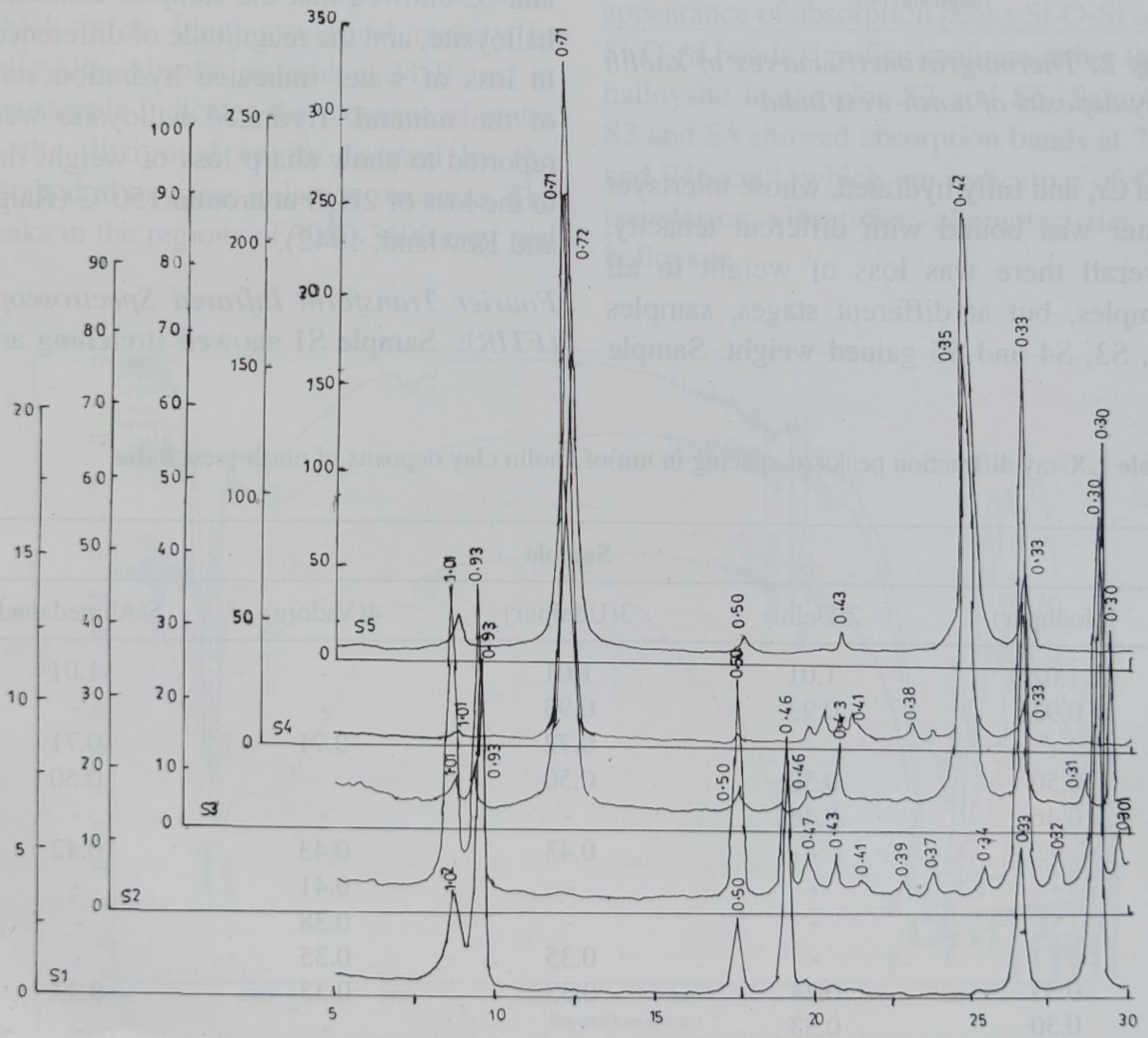

Fig. 1. *X-ray Diffractograms of Clay Deposits of North-West India*

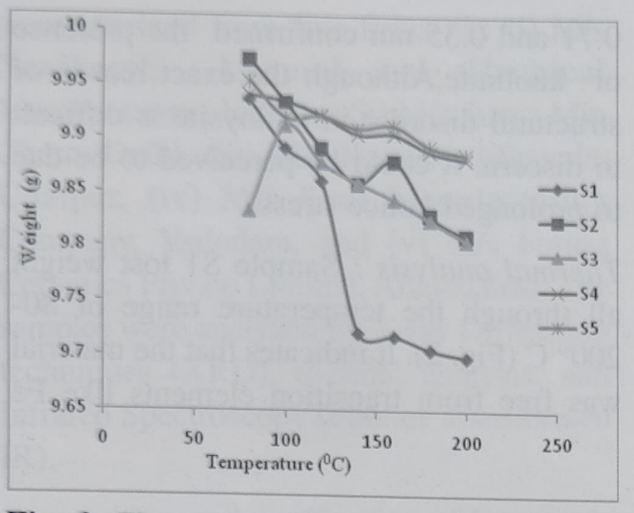

Fig. 2. *Thermogravimetriccurves of kaolin clay deposits of north-west India*

and Cr, and fully hydrated, whose interlayer water was bound with different tenacity. Overall there was loss of weight in all samples, but at different stages, samples S2, S3, S4 and S5 gained weight. Sample S3 gained weight at 100° C, sample S5 at 120° C; and samples S2 and S4 at 160° C. Gain of weight was indicative of oxidation of lower valence state metals like Fe and Mn to their higher valance state. The initial loss of weight between 80 and 110°C was due to loss of hygroscopic water. There was sharp fall of weight around 150° C in S1 followed by S2, while it was modest in S4, and S5. The sharp loss of weight in S1, and S2 showed that the samples contained halloysite, and the magnitude of differences in loss of water indicated hydration state of the mineral. Hydrated halloysite were reported to show sharp loss of weight due to the loss of $2H_2O$ at around 150°C (Ralph and Rowland, 1942).

Fourier Transform Infrared Spectroscopy (FTIR): Sample S1 showed stretching and

Table 1.X-ray diffraction peaks (d-spacing in nm)of kaolin clay deposits of north-west India

Sample				
1(Jodhpur)	2(Delhi)	3(Udaipur)	4(Vadora)	5(Ahmedabad)
1.02	1.01	1.01	-	1.01
0.93	0.93	0.93	-	-
-	-	0.72	0.71	0.71
0.50	0.50	0.50		0.50
0.46	0.46	-	-	-
-	-	0.43	0.43	0.42
-	-	-	0.41	-
-	-	-	0.38	-
-	-	0.35	0.35	-
0.33	0.34	0.33	0.33	0.33
0.30	0.33	-	-	-
-	0.30	0.30	-	-

bending of water at 3450, 1648 and 1629 cm^{-1} (Fig. 3) coupled with stretching, vibration and translation of OH (Table 2). Both absorption bands at 1648 and 1629 cm^{-1} were observed in this sample. Frost (2010) opined that peak at 1648 cm^{-1} was due to water with strong hydrogen bonding, and peak at 1629 cm^{-1} was for water in bending mode without hydrogen bond. These observations confirmed presence of hydrogen bond in the interlayer water sheet, which is an ideal structural moiety in halloysite. Absorption peak at 3450 cm^{-1} in this sample indicates the presence of water in the ditrigonal cavity formed by the tetrahedral oxygens in lattice structure. The peaks in the regions of 3050-3600 cm^{-1} and 1600-1700 cm^{-1} suggest presence of two types of water in the structure that distinguishes halloysite from kaolinite. These data showed that sample S1 consisted of fully hydrated halloysite.

In general, IR bands were observed at 3695, 3676, 3647 and 3620 cm^{-1} frequency in all samples, which were reflective of hydroxyl stretching. Absence of diagnostic absorption peaks in conjunction with appearance of absorption peaks Si-O-Si and Si-O-Al bonds signifies kaolinite rather than halloysite in samples S2 and S5. Samples S3 and S4 showed absorption bands at 796 and 746 cm^{-1}, which are indicative of OH translation vibrations; characteristics of halloysite.

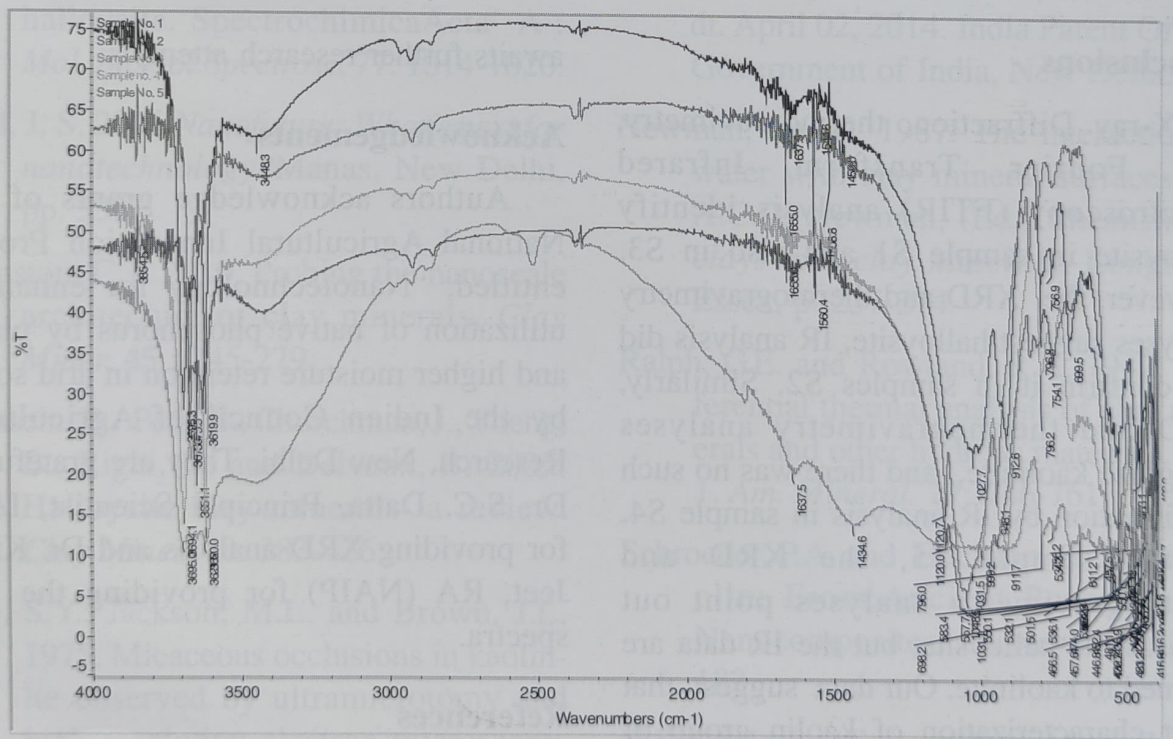

Fig. 3. Fourier Transform Infra Red (FT-IR) spectra of kaolin clay deposits

Table 2. Infra-red absorptionpeaks (in cm^{-1}) of kaolin clay deposits of north-west India

Sr No.	Wave No.	Identification of Peak	S1	S2	S3	S4	S5
1	3695	Inner OH Stretching	*	absent	*	*	absent
2	3676	Out of phase inner OH vibration	absent	*	absent	absent	*
3	3647	Out of phase inner OH vibration	*	absent	absent	absent	absent
4	3620	Inner OH Stretching	*	absent	*	*	absent
5	3450	H_2O stretching	*	absent	absent	absent	absent
6	1648	HOH Bending	*	absent	*	*	absent
7	1629	HOH Bending	*	absent	absent	absent	absent
8	1119	Si-O	absent	*	absent	absent	*
9	1029	Si-O-Si	*	*	absent	*	*
10	998	Si-O-Si	absent	absent	*	absent	absent
11	939	Al-OH Deformation	absent	absent	absent	absent	*
12	912	Inner OH	*	absent	absent	*	absent
13	791	OH Translation	*	absent	*	*	absent
14	747	OH Translation	*	absent	*	*	absent
15	538	Al-O-Si	*	*	*	*	*
16	470	SI-O-Si	*	*	*	*	*
17	436		*	*	*	*	*

Conclusions

X-ray Diffraction, thermogravimetry, and Fourier Transform Infrared Spectroscopy (FTIR) analysis identify halloysite in sample S1 and also in S3. However, the XRD and thermogravimetry analyses suggest halloysite, IR analysis did not confirm it in samples S2. Similarly, XRD and thermogravimetry analyses recognize kaolinite, and there was no such confirmation by IR analysis in sample S4. In the sample S5, the XRD and thermogravimetry analyses point out towards the halloysite, but the IR data are inclined to kaolinite. Our data suggest that exact characterization of kaolin group of minerals remains a still a challenge and awaits further research attempts.

Acknowledgements

Authors acknowledge grants of the National Agricultural Innovation Project entitled, "Nanotechnology for enhanced utilization of native phosphorus by plants and higher moisture retention in arid soils" by the Indian Council of Agricultural Research, New Delhi. They are grateful to Dr. S.C. Datta, Principal Scientist, IARI for providing XRD analysis and Dr. Kiran Jeet, RA (NAIP) for providing the IR spectra.

References

Churchman, G.J. and Theng, B.K.G. 1984.

Interactions of halloysites with amides: mineralogical factors affecting complex formation. *Clay Miner.* **19**: 161-175.

Dixon, J. B. 1989. kaolin and serpentine group minerals. In: Dixon, J.B. and Weed, S.B. (Ed) *Minerals in Soil Environments.* Soil Science Society of America, Madison,Wisconsin, USA, Pp 467-519.

Frost, R.L. 1995. Fourier transformraman spectroscopy of kaolinite, dickite and halloysite. *Clays Clay Miner.* **43** : 191-195.

Frost, R.L., Yang, J., Cheng, H., Liu, Q., He, J. and Unspecified 2010. Infrared and infrared emissionspectroscopic study of China typical kaolinite and halloysite. SpectrochimicaActa A : *Mol. Biomol.Spectrosc.* **77**: 1014-1020.

Hall, J. S. 2006.*Nanofuture: What's next for nanotechnology?*Manas, New Delhi, pp. 333.

Johnston, C.T. 2010. Probing the nanoscale architecture of clay minerals. *Clay Miner.* **45** : 245-279.

Joussein, E., Petit, S., Churchman, J., Theng, B., Righi, D. and Delvaux, B. 2005. Halloysite clay minerals- a review. *Clay Miner.* **40**: 383-426.

Lee, S.Y., Jackson, M.L. and Brown, J.L. 1975. Micaceous occlusions in kaolinite observed by ultramicrotomy and high resolution electron microscopy. *Clays Clay Miner.* **23**: 125-129.

Mukhopadhyay, S.S. 2014. Nanotechnology in agriculture: prospects and constraints. *Nanotechnol. Sci. Appl.***7**:1-9.

Mukhopadhyay, S.S. and Kalia, A. 2014a. Nanofabrication of phosphorous on kaolin receptacle mineral for its use as advanced nanomaterials including novel fertilizer (Products). Provisional Specification # 989/DEL/2014 dt. April 07, 2014. India Patent Office, Government of India, New Delhi.

Mukhopadhyay, S.S. and Kalia, A. 2014b. Nanofabrication process involving clay minerals as receptacles for manufacturing advanced nanomaterials including novel fertilizers (Process). Provisional Specification # 959/DEL/2014 dt. April 02, 2014. India Patent Office, Government of India, New Delhi.

Newman, A.C.D. 1987. The interaction of water with clay mineral surfaces. In: A.C.D. Newman, (Ed.) *Chemistry of clays and clay minerals*. Longman, Essex, p. 237-274.

Ralph, G.E. and Rowland, R.A. 1942. Differential thermal analysis of clay minerals and other hydrous materials. Part 1. *Am. Mineral.* **27**: 746-761.

Schroeder, P.A. and Erickson, G. 2014. Kaolin: From Ancient Porcelains to Nanocomposites. *Elements* **10:** 177-182.

U.S. Geological Survey, 2011, Mineral com-

modity summaries 2011: U.S. Geological Survey, p. 198 *http://minerals.usgs.gov/minerals/pubs/mcs/index.html* Asupdated on: December 20, 2012.

US Environmental Protection Agency. Nanotechnology White Paper. Report EPA 100/B-07/001, Washington DC, USA, 2007. Available from: http://www.epa.gov/osainter/ pdfs/nanotech/epa-nanotechnology-whitepaper-0207.pdf. Accessed June 9, 2014.

(Received January 2015; Accepted May, 2015)

Clay Research, Vol. 33, No. 2, pp. 83-96 (2014)

Potential of Bentonite Clay for Heavy Metal Immobilization in Soil

P. KUMARARAJA[A,B], K.M. MANJAIAH[A*], S.C. DATTA[A] AND T.P. AHAMMED SHABEER[C]

[a]*Division of Soil Science and Agricultural Chemistry, ICAR-Indian Agricultural Research Institute, New Delhi*
[b]*ICAR-Central Institute of Brackishwater Aquaculture, Chennai, Tamil Nadu*
[c]*ICAR-National Research Centre for Grapes, Pune, Maharashtra*

Abstract–*A montmorillonite rich bentonite clay was evaluated for heavy metals (Cu and Zn) removal from aqueous system and its immobilization efficiency of the metals in soil by batch adsorption experiment. The effect of adsorbent amount, pH and initial concentration of metals on the extent of adsorption was investigated. The adsorption data were fitted with Langmuir, Freundlich and Dubinin-Radushkevich adsorption isotherms. The maximum monolayer adsorption capacity of bentonite was obtained from Langmuir adsorption isotherm and its values are 13.95 mg g^{-1} and 11.41 mg g^{-1} for Cu (II) and Zn (II), respectively. The maximum monolayer adsorption capacity of the soil increased from 1.39 mg g^{-1} to 11.76 mg g^{-1} and 0.42 mg g^{-1} to 10.50 mg g^{-1} for Cu (II) and Zn (II), respectively, on addition of bentonite. The study demonstrates that bentonite has potential to remove Cu (II) and Ni (II) ions from aqueous solution and also from heavy metal polluted soil.*

Key words : Bentonite, Heavy metal, Adsorption, Soil

Heavy metal pollution is one of the most serious environmental problems facing modern society and it has received a great deal of attention due to their toxic effect to the ecosystem, agriculture, and human health. Heavy metal contamination in the surface- and ground water environment prevents any beneficial use of the water bodies as well as makes the soil as barren. Therefore, control of heavy metals in waste effluents before its disposal into the environment is essential. Conventional technologies in heavy metal removal include precipitation, ion exchange, reverse osmosis, and filtration (Kurniawan *et al.*, 2006). However, these methods have several disadvantages/limitations such as being expensive, generating secondary pollutants like sludge, and ineffective in treating effluents with low metal

***Corresponding Author :** K.M.Manjaiah, manjaiah@iari.res.in

concentrations etc. Among the physico-chemical treatments, adsorption process is easy to operate and can treat waste effluents with high loadings and at very low concentrations (Bhattacharya and Gupta, 2006a). Continuous application of poor quality irrigation water results in soil as sink and makes it barren. To avoid the transfer of metal from soil to human food chain in-situ immobilization of heavy metals is a promising alternative to the expensive and disruptive conventional ex-situ remediation techniques for the contaminated soil.

Use of clays as adsorbents to remove contaminants has been increasingly paid attention because of their mechanical stability, low cost, availability and presence of metal chelating functional groups and negative charge on surface (Fu and Wang, 2011). In this study bentonite clay was evaluated for their potential heavy metal removal from aqueous system as well as metal sorption capacity of a contaminated soil.

Materials and Methods

Instrumentation

The X-ray diffraction patterns of the bentonite clay was obtained with a diffractometer (Philips PW1710) using Cu K α radiation and scanning from 3° to 15° at a step angle 0.1°, 5 s/step. The specific surface area (SSA) of clays was determined by ethylene glycol monoethyl ether method (Carter *et al.,* 1965) and cation exchange capacity (CEC) by magnesium- calcium replacement method. The SSA and CEC values for normal bentonite were 399 m^2g^{-1} and 83.3 cmol (p^+) kg^{-1}, respectively. The concentration of metal ions was determined by the AAS.

Materials and reagents

Bentonite clay mineral was purchased from Minerals limited, New Delhi, India. Stock solutions of metals (Zn, and Cu) containing 1000 mg L^{-1} metal ion was prepared by dissolving appropriate amount of AR grade sulphate [$Cu(SO_4)_2.5H_2O$; $Zn(SO_4)_2.7H_2O$] salts of heavy metals separately in double distilled water. The working standard solutions of metals were prepared from the stock solution by appropriate dilution using double distilled water. The soil (Aridisol) used in batch adsorption study was collected from Pali, Rajasthan, India. The physico-chemical properties of the contaminated soil used for adsorption study were determined by standard methods.

Adsorption and desorption experiments

All the adsorption equilibrium experiments were conducted by batch method. A known volume (50 mL) of metal solutions of varying initial concentrations (0 to 50 ppm), in polypropylene bottle was shaken with a desired dose of adsorbent for a specified contact time in an end to end shaker. After the pre-determined adsorption time, solution was filtered through Whatman No. 42 filter paper. The

initial and equilibrium concentrations of metal in the aqueous solutions were analysed by atomic adsorption spectroscopy (AAS). The amount of metal adsorbed (Q in mg g^{-1}) was determined as follows:

$$Q = [(C_o - C_t)/m] V$$

Where, Q is the amount of metal ions adsorbed onto unit amount of the adsorbent (mg g^{-1}), C_0 and C_t are the initial and terminal concentrations of metal in solution (mg L^{-1}), V is the volume of solution (L) and m is the mass of the adsorbent (g), respectively. The percentage removal of metal ion was calculated by following equation:

$$\text{Removal (\%)} = [(C_0 - C_t)/C_0] 100$$

where C_0 and C_t are the initial and terminal concentrations of metal in solution (mg L^{-1}).

To study the effect of bentonite clay on heavy metal sorption by soils, one gram soil and 0.1 g of bentonite were taken in 30 ml polypropylene centrifuge tube and shaken for 24 hours in an end to end shaker with 30 ml of metal solution of varying concentration (0-50 ppm). At the end of shaking hour, centrifugation was done at 8000 rpm for 10 minutes and 15 ml of supernatant was withdrawn. To study the desorption 15 ml of 0.01M Ca $(NO_3)_2$ was added to the contents of centrifuge tube and shaken for 24 hours.

The distribution coefficient of an adsorbent is defined as the ratio of the metal ion adsorbed to the amount in the liquid phase. The distribution coefficient was calculated according to the following equation:

$$\text{Distribution coefficient } (K_d, L/g) = [(C_0 - C_t) / C_t] * V / m$$

where, C_0 and C_t are the initial and terminal concentrations of metal in solution (mg L^{-1}), V is the volume of the solution (L) taken and m is the mass of adsorbent (g) taken.

Effect of adsorbent level: To examine the effect of adsorbent level on metal adsorption, 50 ml of 25 ppm metal solution with different amount of bentonite (0.01, 0.025, 0.05, 0.1, and 0.2 g) in polypropylene bottle was shaken for a specified contact time (4 hrs) in an end to end shaker. After the pre-determined adsorption time, solution was filtered with Whatman No.42 filter paper. The initial and equilibrium concentrations of metal in the aqueous solutions were analysed by the AAS.

Effect of pH: To examine the effect of pH on metal adsorption, 50 mL of 25 ppm metal solution with different pH values (1, 2, 3, 4, 5, 6, 7 and 8) and 0.1 g of adsorbent in polypropylene bottle was shaken for a specified contact time in an end to end shaker. After the predetermined adsorption time, solution was filtered with Whatman No.42 filter paper. The initial and equilibrium concentrations of metal in the aqueous solutions were analysed by the AAS.

Results and Discussion

Characterisation of bentonite

Figure. 1 represents the random oriented XRD pattern of the bentonite clay which shows a strong peak at $2\theta = 7.0^{o}$ (d=spacing of 12.2Å) corresponds to smectite mineral. Bentonite sample is mainly composed of montmorillonite with minor amounts of quartz and feldspar. Hazem and Masry (2011) reported the basal spacing of commercial bentonite at 12.1Å. Kloprogge *et al.* (2002) reported 11.5Å to 15Å as basal spacing of bentonite clay depending on the different extent of interlayer water molecules possibility related to the differences in interlayer cation composition.

The scanning electron microscopy (SEM) (Fig. 2) shows that the bentonite with closely associated layers forming a relatively compact lamellar structure and the particles are observed to have layered structure with majority of the platelets have hexagonal and subhedral lamella shapes.

Effect of adsorbent level

Amount of adsorbent is an important parameter which determines adsorption capacity. The data (Fig. 3 a & b) indicate that in all the cases percentage removal of metal increased from 60% to 95%, and 35% to 95%, for Cu (II) and Zn (II), respectively. The increase in percentage of removal as dosage was increased due to the increase in surface area of adsorbent. A higher adsorbent dosage also reflects a greater number of available adsorption sites (Vidal

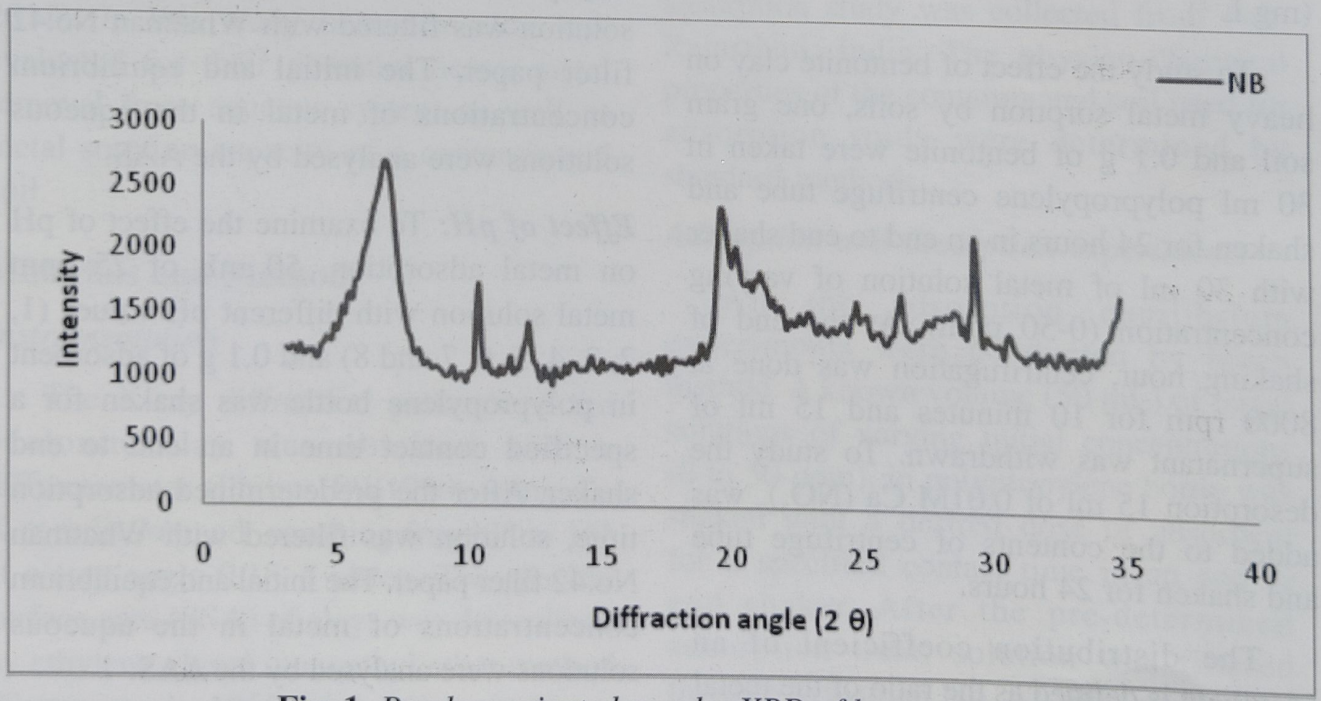

Fig. 1. *Random oriented powder XRD of bentonite clay*

et al., 2009), indicating more metal ions were able to be adsorbed. However reduction in adsorption capacity of bentonite clay with increase in dose of adsorbent was observed for both the metals. As the dosage increased, the ratio of number of adsorption sites to the number of metal ions would increase because fixed amount of metal ions results in more number of unadsorbed sites. At higher adsorbent dose particle aggregation may decrease the total surface area of the adsorbent and leads to lower efficiency of adsorbent.

Effect of pH

The pH of the solution strongly affects the adsorption capacity of bentonite clay. The data (Fig. 4 a & b) indicate that adsorption of metals increases with increasing pH of the solution and maximum adsorption of Cu (II) and Zn (II) occurs at pH 6 and 7, respectively. Lower adsorption of metals at acidic pH is attributed to higher concentration of H^+ and hydronium (H_3O) ions and their competition with metal ions for adsorption sites (Newton *et al.*, 1976) and diminution of the cation exchange capacity (CEC) of the sorbent (bentonite). At pH above isoelectric point the surface becomes negatively charged and the functional groups such as hydroxyl, silanol and aluminol attract metal cation there by resulting in electrostatic interaction. At higher pH metal adsorption increases due to reduced inhibitory effect of H^+. Cu (II)

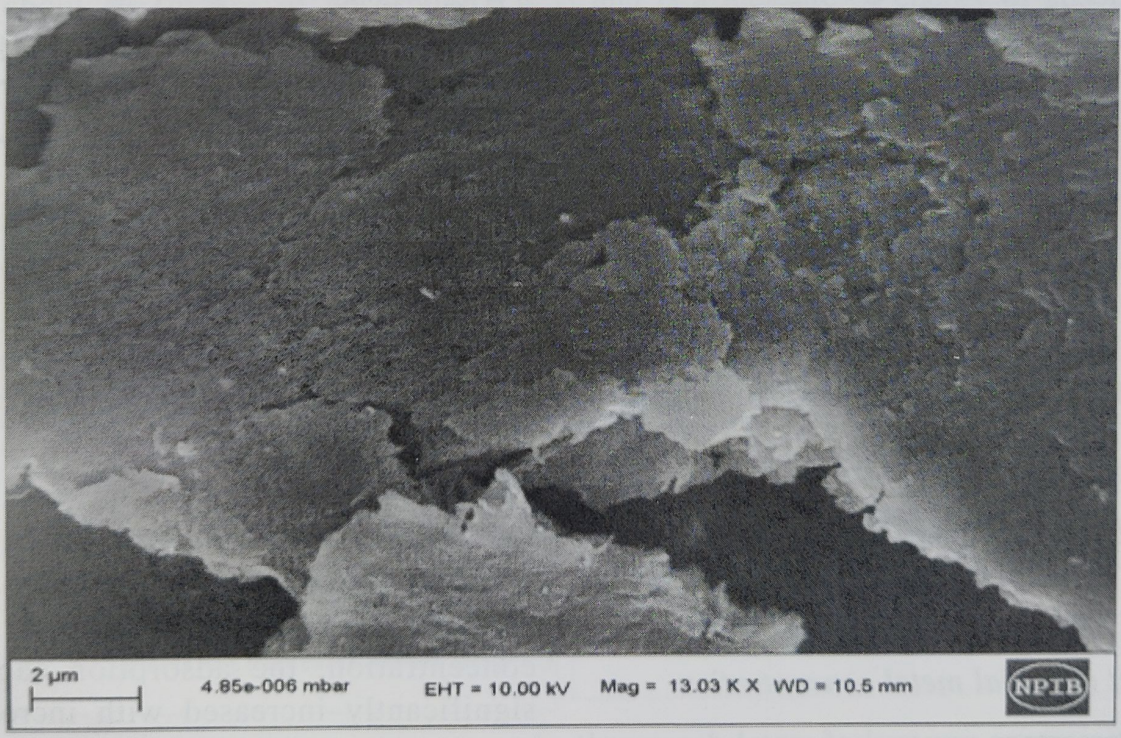

Fig. 2. *Scanning electron micrograph of bentonite clay*

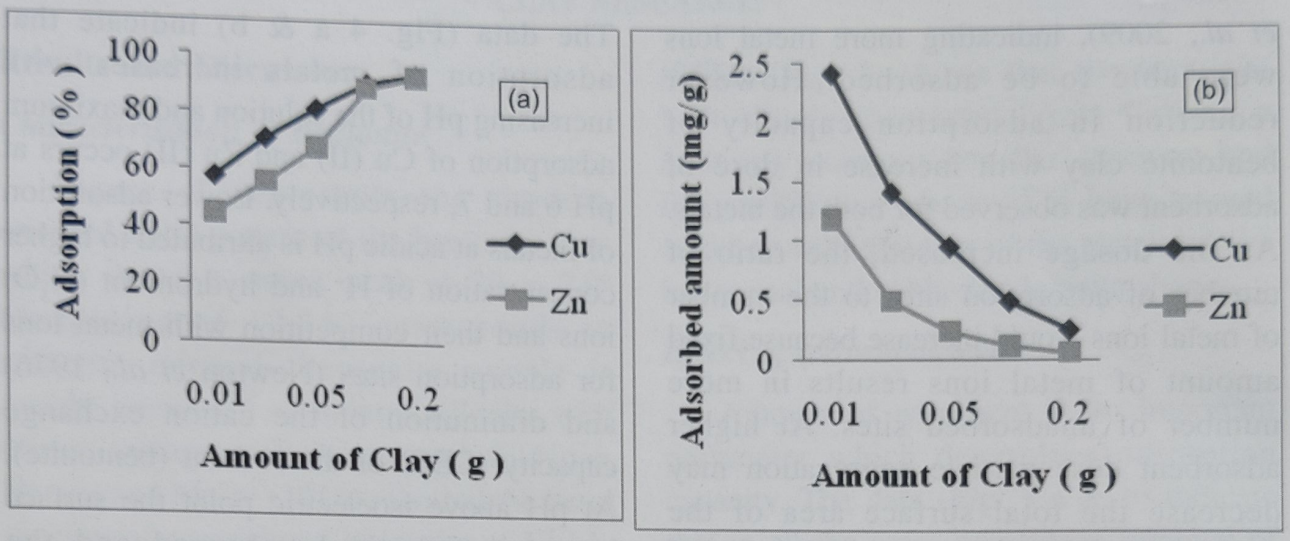

Fig. 3. *Effect of adsorbent dose on percentage removal (a) and amount of metal adsorbed per unit amount of adsorbent (b)*

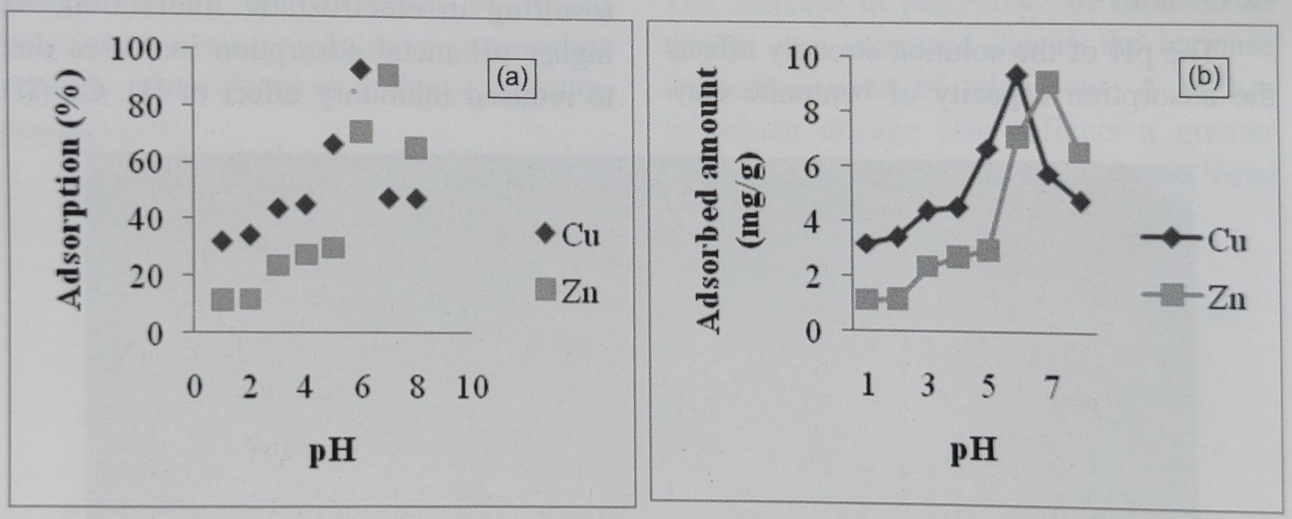

Fig. 4. *Effect of pH on percentage removal (a) and adsorption capacity (mg/g) of bentonite clay (b)*

and Zn (II) get precipitated at pH above 6 and 7, respectively resulted in lower adsorption.

Effect of initial metal concentration

Percentage removal of metal decreased with increase in initial concentration and the reverse trend observed in case of sorption capacity per unit amount of adsorbent (Fig. 5 a & b). At low metal concentration, the adsorption capacity significantly increased with increasing metal concentration because of increased level of metal ions in the solution enhanced

the interactions between metal ions and the active sites of the adsorbent. The initial concentration of metal ions act as an important driving force to overcome all mass transfer resistance of metal ions between the solid and solution phase.

Adsorption isotherms

An adsorption isotherm indicates the mathematical relationship between the adsorption capacity and equilibrium concentration of an adsorbent at a constant temperature. The adsorption data were analysed with the Langmuir, Freundlich and Dubinin-Radushkevich (DR) isotherm models. The Langmuir and Freundlich models are often used to describe the adsorption isotherm. DR isotherm gives the idea about the nature of adsorption i.e. whether it is chemisorption or physi-sorption based on the free energy of adsorption.

The Langmuir equation suggests that the sorption occurs at the solid surface that is made up of elementary sites, each of which can adsorb one sorbate molecule, *i.e.,* monolayer sorption (Langmuir, 1918). The Langmuir equation is given below:

$$Q_e = (Q^o b C_e)/(1+bC_e)$$

The linear version of Langmuir equation is: $C_e / q_e = 1/Q^o b + C_e/Q^o + 1$

Where, Q^o is the maximum adsorption at monolayer (mg g^{-1}), C_e is the equilibrium concentration of metal (mg L^{-1}), q_e is the amount of metal adsorbed per unit weight of composite, b is the Langmuir constant related to affinity of binding site (L mg^{-1}) and is a measure of energy of adsorption. A linearized plot of C_e / q_e against C_e gives Q^o and K_L.

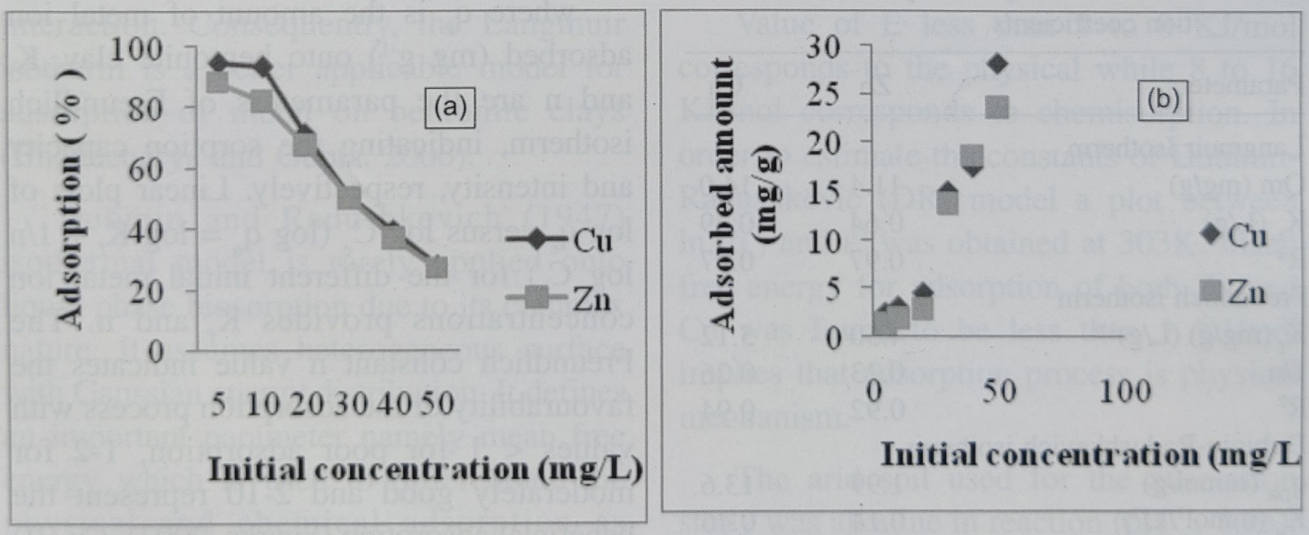

Fig. 5. *Effect of initial concentration on metal adsorption capacity (a) and percentage reomoval of metals (b) by bentonite clay*

Langmuir constant Q^o, represent the maximum monolayer adsorption capacity of the composite. The values are 14.0 mg g^{-1} and 11.4 mg g^{-1} for Cu (II) and Zn (II), respectively (Table 1). Based on the maximum adsorption capacity values the sequence of metal sorption was found to be Cu (II) > Zn (II). This result is in consistent with Ayala *et al.*, (2009) and they reported that the sequence of metal sorption for Peruvian bentonite was Cu (II) > Zn (II) > Ni (II) > Co (II). The high adsorption of Cu (II) ions is due to its paramagneticity, high electronegativity, coordination geometry and Jahn-Teller distortion (Vidal *et al.*, 2009). The sequence of Q^o was consistent with the first hydrolysis constants (K_h) of the metals studied i.e., Cu ($10^{-7.7}$) and Zn ($10^{-9.2}$). Metals with larger K_h (lower pK_h values) form surface hydroxy species within given pH range and are chemisorbed to the surface to a greater extent. Greater adsorption of Cu than that Zn might be due to precipitate phase formation by Cu on the clay surfaces (Hui *et al.*, 2005). The sequence of Q^o was positively correlated with the hardness of metals (5.55 and 5.40 for Cu and Zn, respectively). Degree of hardness shows the polarizability of the metal cation and its affinity for ligands. Higher the hardness, more the affinity to surface functional groups such as mineral – OH groups resulted in higher adsorption of Cu (Sparks, 2003).

Table 1. Isotherm constants for metal sorption on bentonite in aqueous system and correlation coefficients

Parameters	Zn	Cu
Langmuir Isotherm		
Qm (mg/g)	11.4	14.0
K_L (L/g)	0.64	0.29
R^2	0.97	0.97
Freundlich isotherm		
K_f (mg/g) $(L/g)^{1/n}$	4.50	5.12
1/n	0.23	0.26
R^2	0.92	0.94
Dubinin-Radushkevich isotherm		
q_{DR} (mmol/g)	1.99	13.6
K_d ($mmol^2/kJ^2$)	0.14	0.46
E (kJ/mol)	0.54	0.96
R^2	0.94	0.89

The Freundlich (1906) isotherm is an empirical equation and is one of the most widely used isotherms for the description of multi-site adsorption where the adsorbent surface is heterogeneous in nature. Mathematically, it is expressed as

$$q_e = K_f \times C^{1/n}$$

where q_e is the amount of metal ion adsorbed (mg g^{-1}) onto bentonite clay. K_f and n are the parameters of Freundlich isotherm, indicating the sorption capacity and intensity, respectively. Linear plots of log q_e versus log C_e (log q_e = log K_f + 1/n log C_e) for the different initial metal ion concentrations provides K_f and n. The Freundlich constant n value indicates the favourability of the adsorption process with values < 1 for poor adsorption, 1-2 for moderately good and 2-10 represent the beneficial adsorption (Sparks, 2003). Cu (II) has the larger K_f and n values over Zn (II) (Table 1). Cu (II) with the highest n value

means it has highest affinity towards the functional groups of the composite and stronger bond results in higher K_f. According to Freundlich adsorption theory, the n values between 1 and 10 indicate beneficial adsorption, and in this study the n values are more than unity for both the metals which demonstrates the beneficial adsorption. The correlation values (Table 1) of adsorption isotherms indicate that Langmuir isotherm fits better than Freundlich. The Freundlich adsorption isotherm considers the surface heterogeneity of surface and the exponential distribution of the active sites, as well as their energies. On the other hand, Langmuir adsorption model is based on the assumption of a sorption on homogeneous surface by monolayer adsorption, while considering no interaction between adsorbed species. Moreover, Langmuir model assumes that the adsorptive forces are similar to the forces of the chemical interaction. Consequently, the Langmuir isotherm is a better applicable model for adsorption of metal on bentonite clays (Bhattacharya and Gupta, 2006).

Dubinin and Radushkevich (1947) isothermal model is rarely applied onto liquid phase biosorption due to its complex nature. It assumes heterogeneous surface with Gaussian energy distribution. It defines an important parameter namely mean free energy which is used to differentiate the physical and chemical adsorption as follows:

$$q_e = q_{DR}\exp(\text{“}k_d\,\varepsilon^2)$$

where, k_d ($mol^2.kJ^{-2}$) is the constant related to the calculated average sorption energy E, and q_{DR} ($mol.g^{-1}$) is the maximum adsorption capacity which can be calculated respectively from the slope and intercept of following linearized equation:

$$\ln q_e = \ln q_{DR}\ \text{“}k_d\,\varepsilon^2$$

The polyanic potential å can be calculated by the following expression:

$$\varepsilon = RT\ln(1+1/C_e)$$

where, k_d represents adsorption energy and q_{DR} is the maximum adsorption capacity of adsorbent. As an index of consumed energy in adsorption, E represents the free energy per mol of metal ion transferring from infinity in solution to the adsorbent surface k_d is used to estimate mean free energy by the following expression:

$$E = 1/(2\,k_d)^{0.5}$$

Value of E less than 1 to 8 KJ/mol corresponds to the physical while 8 to 16 KJ/mol corresponds to chemisorption. In order to estimate the constants of Dubinin-Radushkevic (DR) model a plot between ln (q_e) and ε^2 was obtained at 303K. Mean free energy for adsorption of both Zn and Cu was found to be less than 1 KJ/mol implies that adsorption process is physical mechanism.

The arid soil used for the adsorption study was alkaline in reaction ($pH_{1:2}$-8.95), sandy in texture with organic carbon

content of 2.43 g/kg and CEC of 9.2 (cmol(p^+) kg^{-1}) (Table 2). Effect of bentonite addition on soil metal sorption was described by the most commonly used isotherms such as Langmuir and Freundlich. Both Langmuir and Freundlich models described the sorption data best for both the metals on soil based on the correlation coefficient (Table 3). Langmuir constant Q^o, represent the maximum monolayer adsorption capacity of soils. The values are 1.08 mg g^{-1} and 1.39 mg g^{-1} for Zn (II) and Cu (II), respectively for arid soil. Based on values of the maximum adsorption capacity calculated from the fitted Langmuir equations the sequence of metal sorption was greater for Cu (II) than Zn (II). The maximum monolayer adsorption capacity of the soil treated with the bentonite clay was 10.5 mg g^{-1} and 11.76 mg g^{-1} for Zn (II) and Cu (II), respectively. The higher adsorption of Cu than that of Zn might be due to its higher relative binding strength, electronegativity and hydrolysis constant and lower ionization potential. The maximum adsorption capacity of soil for Zn (II) and Cu (II) increased in presence of the bentonite than that of untreated soil. This might be due to the increased adsorption sites available for the metals in presence of the bentonite. Application of bentonite increased the monolayer maximum adsorption capacity of soil by 8.5 fold and 9.7 fold for Cu and Zn, respectively. Similar findings are reported

Table 2. Basic physical and chemical properties of the soil used in adsorption study

Mechanical composition	
Sand (%)	67.1
Silt (%)	22.1
Clay (%)	10.9
Soil Texture	Sandy
pH (1:2)	8.95
EC (1:2) (dSm^{-1})	1.09
CEC (cmol(p^+) kg^{-1})	9.2
Soil organic carbon (g kg^{-1})	2.43
Available soil N (mg kg^{-1})	85
Available soil P (mg kg^{-1})	3.8
Available soil K (mg kg^{-1})	102
DTPA extractable	
Zinc (mg kg^{-1})	0.5
Copper (mg kg^{-1})	0.2
Nickel (mg kg^{-1})	Nd

Table 3. Isotherm constants for metal sorption on soil in presence and absence of bentonite and correlation coefficients

Parameters	Zn	Cu
Langmuir Isotherm		
Arid soil		
Qm (mg/g)	1.08	1.39
K_L (L/g)	0.11	0.15
R^2	0.95	0.99
Arid soil + Bentonite		
Qm (mg/g)	10.5	11.76
K_L (L/g)	0.62	0.52
R^2	0.95	0.99
Freundlich isotherm		
Arid soil		
K_f (mg/g) $(L/g)^{1/n}$	0.12	0.18
1/n	0.43	0.7
R^2	0.96	0.97
Arid soil + Bentonite		
K_f (mg/g) $(L/g)^{1/n}$	3.72	2.27
1/n	0.63	0.64
R^2	0.95	0.99

by authors that application of clay minerals (including vermiculite also) enhances the metal sorption capacity of the soils (Xiong *et al.*, 2005; Xiong *et al.*, 2005).

The Freundlich parameter K_f and n values are 0.12, 0.18 for Zn and Cu, respectively and 3.72, 2.27 respectively for soil unamended and amended soil. The n value for both the metals studied was greater than 1, reflecting a favourable adsorption.

The distribution coefficient (K_d) is a useful index for comparing the sorptive capacities of materials for a particular ion under the same experimental conditions (Alloway, 2008). Therefore, a further analysis of the data based on the distribution coefficients was done. The distribution coefficient (K_d) has been calculated over all the initial concentrations of heavy metals (Fig. 6). It is defined as the ratio of the metal concentration in the solid phase to that in the equilibrium solution after a specified reaction time. A high K_d value indicates a higher' metal retention by the adsorbent through sorption and chemical reactions. However, a low K_d value indicates a high amount of the metal remains in the solution. Over all initial concentrations of heavy metals, the highest K_d values were found for Cu and followed by those of Zn (Fig. 6). The results also indicated that the K_d value decreased with increasing the initial metal concentration. This indicates that changes occur in the nature of the sites that are involved in the sorption process, depending upon the metal concentration. The higher K_d value that was obtained in the experiment with lower metal concentrations is associated with the sorption sites of high selectivity, which have

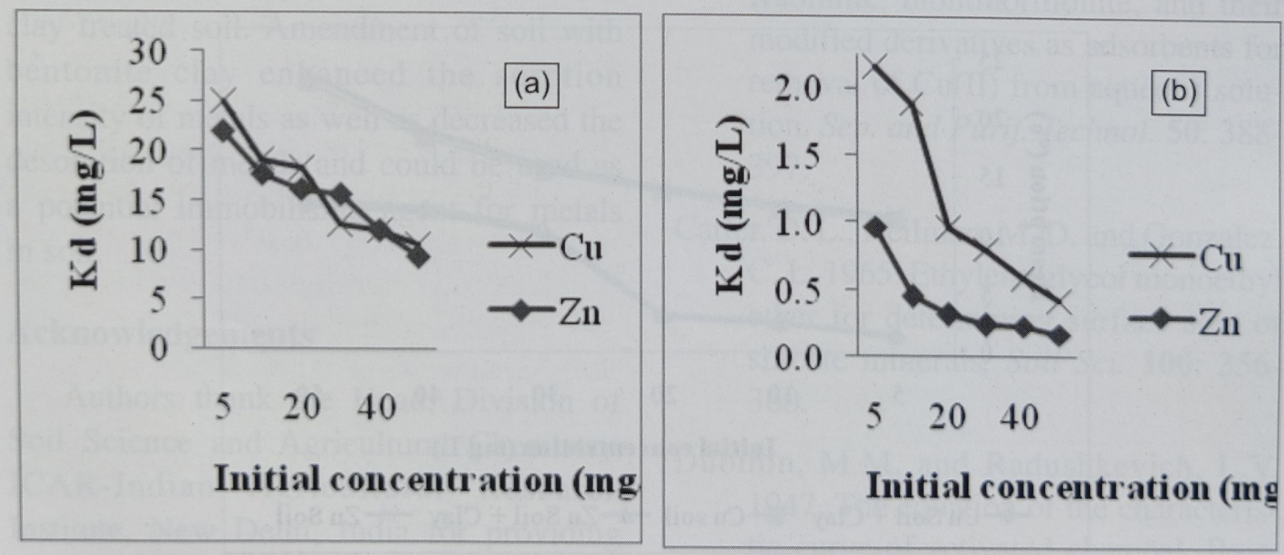

Fig. 6. *Distribution coefficients of Cu and Zn in soil (a) with bentonite and without (b) bentonite clay*

relatively strong bonding energies. Otherwise, heavy metal sorption becomes unspecific at higher metal concentrations, when the specific bonding sites become increasingly occupied, resulting in lower K_d values (Abidin and Kahan, 2005). Higher the K_d value for Cu indicate large affinity of soil with and without the bentonite. From the study it is clear that application of bentonite had positive impact on the metal adsorption capacity of the soil. The higher K_d value in the amended soil indicate that application of bentonite provide additional adsorption sites for the metals in the form of chelating functional groups.

The desorption rate can be used to characterize the degree of metal binding to the adsorbent. Higher the percentage of desorption, the more the loose binding. The desorption of the metals were decreased in presence of bentonite clay from the soil compared to non-treated soil (Fig. 7) indicating the amended soil has more potential to retain the metals than that of untreated soil. This might be due to the strong binding of metals by the functional groups of the bentonite clay. The desorption percentage was higher at higher metal loading for both the metals from the soil both in presence and absence of bentonite. The desorption percentage at all initial concentration was lower for strongly adsorbed metal Cu (0.02% at 5 ppm to 0.27% at 50 ppm) than that of Zn (0.07% at 5 ppm to 3.03% at 50 ppm) in treated soil. The percentage desorption sequence followed the same trend in non-treated soil. The lower percentage of desorption of Cu might be formation of strong complexes with the bentonite clay and at higher loading the desorption might be due to

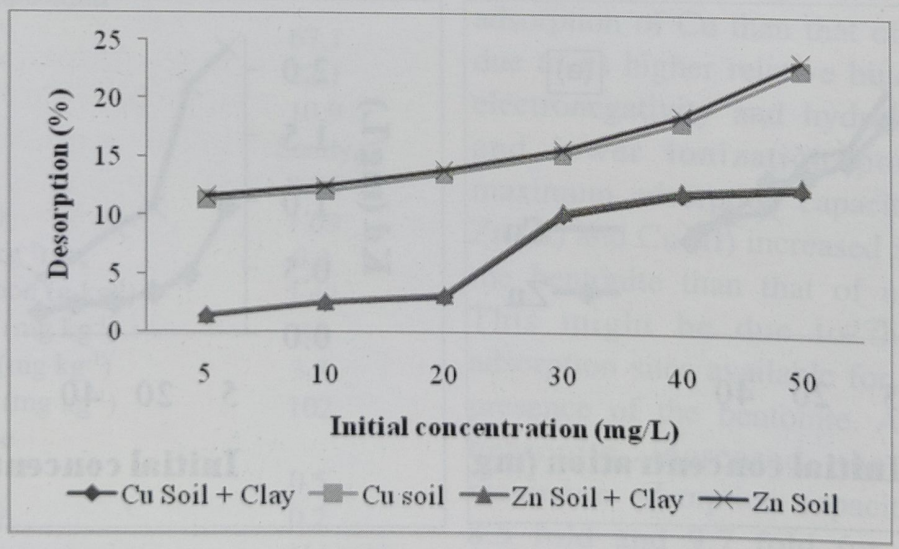

Fig. 7. *Percentage desorption of Cu and Zn from soil (a) with bentonite and without (b) bentonite clay*

sorption at edges of composite. For the loosely bound metals the mechanism might be of ion exchange which resulted in higher desorption percentage.

Conclusion

The effect of adsorbent level, initial metal concentration and pH on metal sorption capacity of bentonite clay showed maximum sorption of Cu and Zn at pH 6 and 7, respectively. The percentage removal of metal decreased with increase in initial concentration and the reverse trend observed in case of sorption capacity per unit amount of adsorbent. Amongst the adsorption isotherms, Langmuir equation fitted well and the study demonstrated the usefulness of bentonite in removal of metals from aqueous solution by adsorption mechanism. Freundlich sorption model fitted well the sorption data of bentonite clay treated soil. Amendment of soil with bentonite clay enhanced the sorption intensity of metals as well as decreased the desorption of metals and could be used as a potential immobilising agent for metals in soil.

Acknowledgements

Authors thank the Head, Division of Soil Science and Agricultural Chemistry, ICAR-Indian Agricultural Research Institute, New Delhi, India for providing all the required facilities to carry out the present investigation.

References

Abidin. K. and Hakan, O.A., 2005. Adsorption of zinc from aqueous solutions to bentonite. *J. Hazard. Mater.* **125**: 183-189.

Alloway, B.J. 2008. *Soil processes and the behaviour of metals. Heavy Metals in Soils*; Alloway, B.J. Ed.; Blackie Academic & Professional, London, p.11–37.

Ayala, J., Vega, J.L., Alvarez, R. and Loredo, J. 2009. Retention of heavy metal ions in bentonites from Garu Region (Northern Peru). *Environ.Geo.* **53**: 1323-1330.

Bhattacharya, K.G. and Gupta, S.S. 2006a. Adsorption of few heavy metals on natural and modified kaolinite and montmorillonite. A review. Adv. *Colloid Inter. Sci.* **140**: 114-131.

Bhattacharya, K.G. and Gupta, S.S. 2006b. Kaolinite, montmorillonite, and their modified derivatives as adsorbents for removal of Cu(II) from aqueous solution. *Sep. and Purif. Technol.* **50**: 388-397.

Carter, D. L., Heilman, M. D. and Gonzalez, C. L. 1965. Ethylene glycol monoethyl ether for determining surface area of silicate minerals. *Soil Sci.* **100**: 356-360.

Dubinin, M.M. and Radushkevich, L.V. 1947. The equation of the characteristic curve of activated charcoal. Proc. Acad. Sci. *USSR Phy. Che. Sect.* **55**: 327-329.

Freundlich, H.M.F. 1906. Over the adsorption in solution. *J. Phys. Chem.* **57**: 385-471.

Fu, F. and Wang, Q. 2011. Removal of heavy metals from wastewater: A review. J. *Envir. Manage.* **91**: 407-418.

Hazem E.S. and Masry, M.E. 2011. Superabsorbent nanocomposite hydrogels based on intercalation of chitosan into activated bentonite. *Polym. Bull.* **66**: 721-734.

Hui, K.S., Chao, C.Y.H. and Kot, S.C. 2005. Removal of mixed heavy metal ions in wastewater by zeolite 4A and residual products from recycled coal fly ash. *J. Hazard. Mater.* **127**: 89-101.

Kloprogge, J.T., Evans, R., Hickey, L., and Frost, R.L. 2002. Characterisation and Al-pillaring of smectitites from miles, Queensland (Australia). *Applied Clay Science*, **20** (4-5) : 157-163.

Kurniawan, T.A., Chan, G.Y.S., Lo, W.H. and Babel, S. 2006. Physico-chemical treatment techniques for wastewater laden with heavy metals. *Chem. Eng. J.* **118**: 83–98.

Langmuir, I. 1918. The adsorption of gases on plane surfaces of glass, mica and platinum. *J. Am. Chem. Soc.* **40**: 1361-1403.

Newton, D.W., Ellis, R. Jr. And Paulsen, G.M. 1976. Effect of pH and complex formation on mercury (II) adsorption on bentonite. *J. Environ. Qual.* **5**: 251-255.

Sparks, D.L. 2003. Environmental Soil Chemistry, 2nd Ed. Academic Press., Elsevier Science, USA.

Vidal, M., Santos, M.J., Abrao, T., Rodriguez, J. and Rigol, A. 2009. Modelling competitive metal sorption in a mineral soil. *Geoder.* **149**: 189-198.

Xiong, X., Stagnitti, F., Allinson, G., Turoczy, N., Li, P., LeBlanc, M., Cann, M.A., Doerr, S.H., Steenhuis, T.S., Parlange, J-Y., Rooif, D. D., Ritsema, C.J., and Dekker, W.L. 2005. Effect of clay amendments on adsorption and desorption of copper in water repellent soils. *Aust. J. Soil Res.* **43**: 397-402.

Xiong, X., Stagnitti, F., Turoczy, N., Allinson, G., Li, P., Nieber, J., Steenhuis, T.S., Parlange, J-Y., LeBlanc, M., Ziogas, A.K., Ferreira, A.J.D and Keizer, J.J. 2005. Competitive sorption of metals in water repellent soils: Implications for irrigation recycled water. *Aust. J. Soil Res.* **43**: 351-356.

(Recieved April 2015 Accepted June 2015)

Clay Research, Vol. 33, No. 2, pp. 97-109 (2014)

Geotechnical and Mineralogical Studies on Edaphic Stresses of the Deccan Trap Formations at NIASM Site, Malegaon, Baramati, Maharashtra

U.K. MAURYA*

National Institute of Abiotic Stress Management (NIASM), Baramati, Pune, Maharashtra - 413115

Abstract: Geotechnical study on 17 Bore Logs with depth up to 5m were conducted at Upper reaches of watershed using rotary drilling rig at NIASM Site, Malegaon, Baramati to understand the nature of lithological / mineralogical compatibility, hydrothermal/ secondary mineral crystallization of individual drill core by measuring the rock strength and assessing their feasibility for the foundation of different building blocks as well as for evaluating the possible role of edaphic stresses. Study indicated two phases of volcanic activity with variable thickness of vesicular and non-vesicular flows and most variable physical parameters are the saturated crushing strength and water absorption due to the inhomogeneous and fractured / altered nature of rocks in different horizons and at variable depths at logging site. Net safe bearing capacity is low in the vesicular flow due to presence of amygdales whereas it is high in non-vesicular flow due to compactness indicating that with diverse lithology the different treatment for the foundations are required to set up a strong base of different blocks.

Assessment of the subsoil strata from safe bearing capacity point of view, geotechnical investigation of soils and rocks using core samples up to depth of 5m were carried out to measure the rock strength of different flow activity, their mineralogical make up and the edaphic stresses if any. Study on the textural and mineralogical composition of Basalts and associated rocks of the region was studied by Kanegaonkar and Powar (1978), Kale and Rajaguru (1987), Kale, *et. al.* (1993), Godbole, *et al.* (1996), Geological Survey of India (1998) and Duraiswami (2009).

Site is located between 18°09" 18.86" N to 74°30'01.33" at Malegaon Khurd, Baramati in Pune District of Maharashtra State in the semi-arid tract of the plains of the Western Ghats with the elevation varying from 547 to 565m MSL. (Fig.1).

***Present address:** Division of Soil Science and Agronomy, Central Soil & Water Conservation Research & Training Institute, 218-Kaulagarh Road, Dehradun, Uttarkhand- 248 195
E-mail: uk_maurya63@yahoo.co.in

Fig. 1. *Google Map of the NIASM site showing the location of the Bore Hole (BH1-17)*

Material and Methods

Drilling and sampling of seventeen boreholes in soil and rock was carried out on the Upper reaches of NIASM watershed. Borehole in soil was advanced using rotary drilling method, while NX size double tube core barrel with diamond bit was used to drill in rock. Water was circulated to cool the drilling bit. Ground water table was recorded after 24 hours of completion of drilling. On completion of drilling, soil samples were packed in plastic containers with proper identification tags. Rock cores were numbered and kept in core boxes. Representative soil and rock samples of Bore Logs were analysed for their various geotechnical properties using standard procedures of Terzaghi *et al.,* (1996) and Coduto, *et al.,* (2011). Chemical analysis of soil and water of few representative samples were carried out as per established laboratory techniques.

Thin section of representative core samples was prepared and studied using petrographic microscope (Nikon, Model No ECLIPSE E200POL) at Pune University using NIS-Element F3.0 and Coral PHOTO-PAINT X3 software to know the textural and mineralogical composition as well as alterations / transformation effects in basalts. Minerals were identified following standard procedure of Read (1963) and Ker (1977). Nature of Bore Logs with mineralogical composition were studied and described as per with standard norms.

Results

Field Study

Bore Hole Observations

The details of each location, its depth and other relevant information are given in the table 1, which indicate that coring depth varies as per with geological formations of the site and bore hole location.

Subsoil Profile

Four types of strata are encountered at the most of the sites as given below.

Stratum I: Silty / Loamy sand.

Stratum II: Highly disintegrated rock recovered as gravely loamy sand mixed with boulders (hard muram).

Stratum III: Highly to moderately weathered hydro-thermally altered (HTA), fine grained amygdaloidal basalt / with some zeolitic cavities, highly to moderately fractured weathered basalt.

Table 1. Location of Bore Hole, depth of coring in soil and rock

Bore Hole No.	Depth in soil (m)	Coring in rock (m)
BH1	0.20	4.80
BH2	0.00	5.00
BH3	0.00	5.00
BH4	0.15	4.85
BH5	0.20	4.80
BH6	0.15	4.85
BH7	0.20	4.80
BH8	0.00	5.00
BH9	0.15	4.85
BH10	0.00	5.00
BH11	0.10	4.90
BH12	0.15	4.85
BH13	0.00	5.00
BH14	0.00	5.00
BH15	0.00	5.00
BH16	0.15	4.85
BH17	0.15	4.85

Stratum IV: Fresh to moderately weathered hydro-thermally altered (HTA) fine grained compact basalt / fine grained grayish compact basalt/ grayish amygdaloidal basalt/ HTA amygdaloidal basalt with some zeolitic cavities.

Thickness of each layer encountered along with RQD (Rock Quality Designation) range as the case may be at the locations is given in table 2. It shall be noted that the stratum listed below may not be encountered in the same order as listed.

The lithological / mineralogical details of individual drill core have been described and a representative of each type i.e. vesicular and non-vesicular flow have been shown in figures 2 and 3 and the details of core recovery (CR), RQD and other parameters are given in the bore logs (Figs. 4-5).

The observed Bore Holes were correlated with respect to their contour height and flow type (Table 3). From the table it is observed that contour height of different Bore Hole differ from 98 to 107m indicating that they have different phases of flow with variable lithological make up. With the above lithological information on the individual drill core, all the seventeen bore logs were correlated to understand the nature of flow, their compatibility and mineralogical composition.

Water Level

During the boring water level was encountered in some of the boreholes as stated below in table 4. This may be for a shorter period. The correct method to determine ground water table is to install standpipe piezometer and monitor over a long period of time.

Laboratory Study

Representative Drill Core samples were selected and classified for the different laboratory testing / investigations as stated below:

Rock samples

Rock samples were tested for different geotechnical parameters to assess their feasibility for the foundation of different

Table 2. Thickness of each layer with RQD

BH No	Layer I	Layer II	Layer III		Layer IV	
	Thick (m)	Thick (m)	Thick (m)	RQD %	Thick (m)	RQD %
BH-1	0.20	-	-	-	4.80	77-96
BH-2	-	-	-	-	5.00	73-85
BH-3	-	-	-	-	5.00	58-99
BH-4	0.15	-	-	-	4.85	87-89
BH-5	0.20	-	-	-	4.80	48-83
BH-6	0.15	-	-	-	4.85	42-81
BH-7*	0.20	-	-	-	4.50	50-79
BH-8	-	0.50	0.30	0	4.20	54-93
BH-9	0.15	1.35	1.00	0	2.50	32-95
BH-10	-	1.50	2.00	0-54	1.50	85
BH-11	0.10	1.40	1.50	0	2.00	56-74
BH-12	0.15	0.85	-	-	4.00	46-70
BH-13	-	-	-	-	5.00	39-58
BH-14	-	1.00	3.00	0-28	1.0	66
BH-15	-	-	2.00	0-23	3.00	45-87
BH-16	0.15	0.10	4.85	0-54	-	-
BH-17	0.15	0.70	1.70	0-39	2.50	59-72

*Layer III encountered below layer IV from 2.2m to 5m

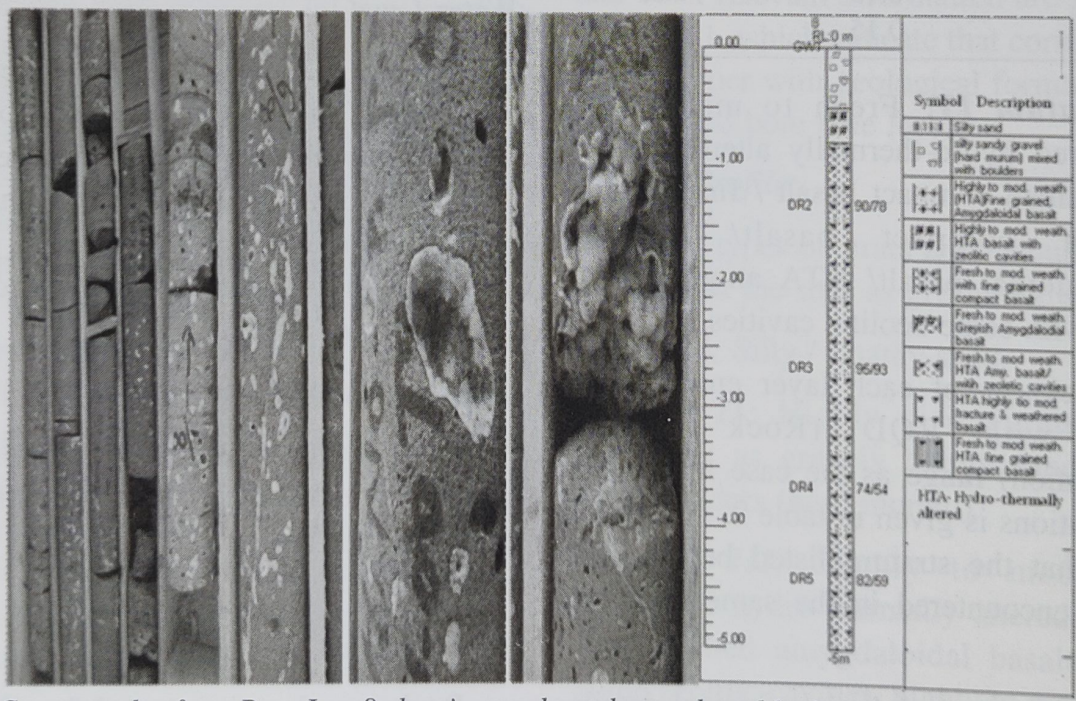

Fig. 2. *Core samples from Bore Log 8 showing moderately weathered hydrothermally altered vesicular basalt of 4.2m thick. The core is characterized by an enriched zone of 0.3m thick well crystallized zeolite just below the gravel and boulder horizon. The upper most layer is the soil horizon of 0.5m thick.*

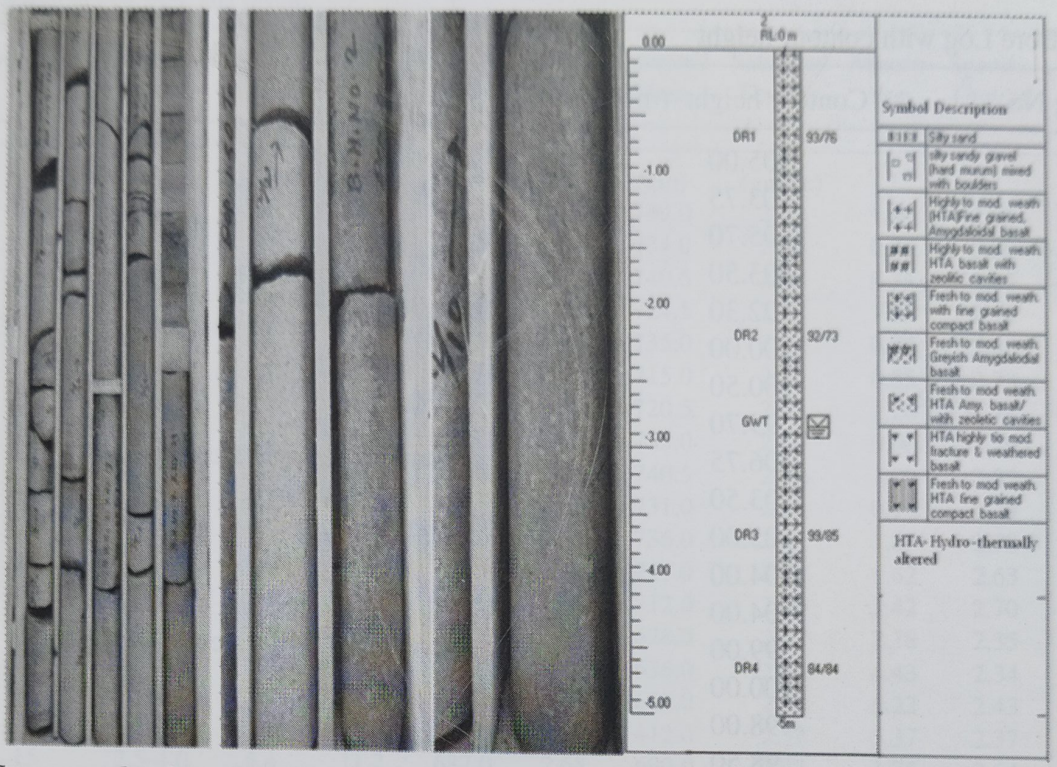

Fig. 3. *Core samples from Bore Log 2 showing moderately weathered fine grained compact basalt from non-vesicular flow of 5m thick.*

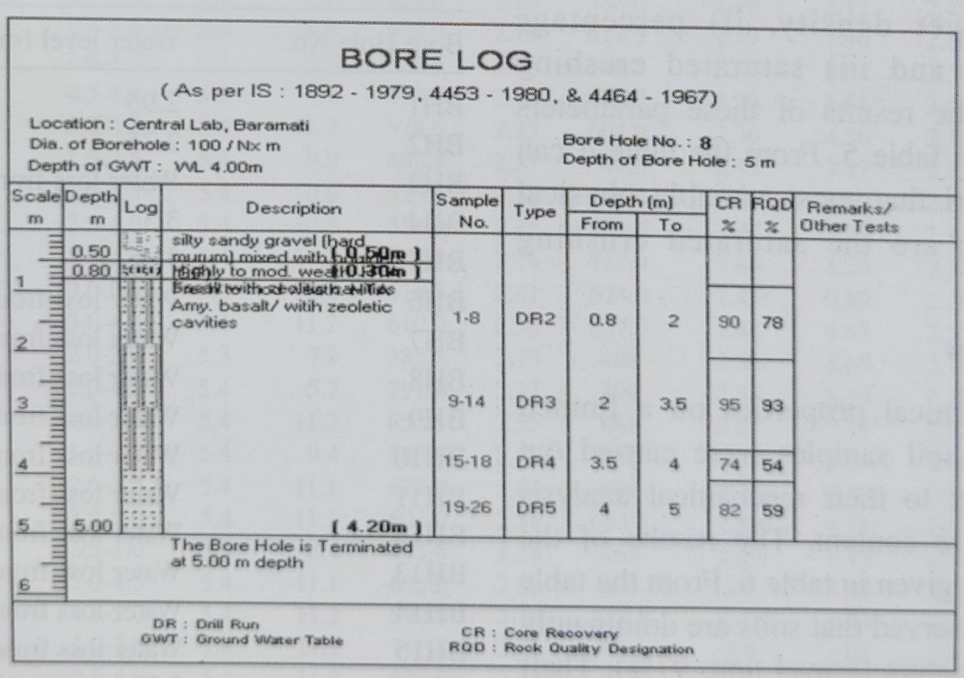

BORE LOG

(As per IS : 1892 - 1979, 4453 - 1980, & 4464 - 1967)

Location : Central Lab, Baramati
Dia. of Borehole : 100 / Nx m
Depth of GWT : WL 4.00m

Bore Hole No. : 8
Depth of Bore Hole : 5 m

Scale m	Depth m	Log	Description	Sample No.	Type	Depth (m) From	Depth (m) To	CR %	RQD %	Remarks/ Other Tests
	0.50		silty sandy gravel (hard murum) mixed with boulders (0.50m)							
	0.80		Highly to mod. weath. (HTA)Fine grained, Amygdaloidal basalt with zeolitic cavities (0.30m)							
1			Fresh to mod. weath. HTA Amy. basalt/ with zeoletic cavities	1-8	DR2	0.8	2	90	78	
2										
3				9-14	DR3	2	3.5	95	93	
4				15-18	DR4	3.5	4	74	54	
5	5.00		(4.20m)	19-26	DR5	4	5	82	59	
6			The Bore Hole is Terminated at 5.00 m depth							

DR : Drill Run
GWT : Ground Water Table
CR : Core Recovery
RQD : Rock Quality Designation

Fig. 4. *Bore log characteristics indicating %RQD and %CR of layer I - IV with depth in vesicular flow of Bore Hole No. 8*

Table 3. Bore Log with contour height

Bore Log No.	Contour height (m)	Flow type
BH1	105.00	Nonvesicular
BH2	103.75	
BH4	105.70	
BH5	103.50	
BH8	102.30	Vesicular
BH10	100.00	
BH11	100.50	
BH14	99.70	
BH3	106.75	Nonvesicular - Vesicular
BH6	103.50	
BH7	105.00	
BH16	104.00	
BH17	104.00	
BH9	99.00	Vesicular - Nonvesicular- Vesicular
BH12	100.00	
BH13	98.00	
BH15	98.50	

building blocks. The most common are i) dry and wet density, ii) percentage absorption and iii) saturated crushing strength. The results of these parameters are given in table 5. From the table it can be observed that most variable physical parameters are the saturated crushing strength.

Soil samples

Geotechnical properties on a limited number of soil samples were carried out with respect to their mechanical analysis and moisture content. The results of the analysis are given in table 6. From the table it can be observed that soils are dominantly gravely in nature (gravel upto 97%). Their moisture content varies with location of logging core.

Table 4. Bore hole number with water level

Bore Hole No.	Water level (m)
BH1	2.95
BH2	2.75
BH3	Water loss from 4.5m
BH4	3.3
BH5	3.45
BH6	Water loss from 4m
BH7	Water loss from 2m
BH8	Water loss from 4m
BH9	Water loss from 4.5m
BH10	Water loss from 3.25m
BH11	Water loss from 4.5m
BH12	Water loss from 4m
BH13	Water loss from 4m
BH14	Water loss from 3m
BH15	Water loss from 5m
BH16	2.85m
BH17	2.9m

Table 5. Summary of rock test results

BH No	Piece No	Depth below GL	Diameter	Height	Dry mass	Dry Density	Saturated Mass	Saturated Density	Absorp-tion	Specific Gravity	Saturated Crushing Strength
		(m)	(cm)	(cm)	(gm)	gm/cc	(gm)	(gm/cc)	?		kg/cm^2
1	4	0.2-1.5	5.4	11.2	741.0	2.89	749.0	2.92	1.08	2.85	588.93
1	15	3.0-4.5	5.4	11.2	728.0	2.84	734.0	2.86	0.82	2.80	679.51
2	3	0.0-1.5	5.4	11.2	735.0	2.87	740.5	2.89	0.75	2.83	815.43
2	23	3.0-4.5	5.4	11.2	711.5	2.78	724.5	2.83	1.83	2.74	135.92
3	4	0.7-1.5	5.4	11.2	729.0	2.84	735.0	2.87	0.82	2.80	679.51
3	19	3.0-4.5	5.4	11.2	709.0	2.77	715.0	2.79	0.85	2.73	362.42
4	6	0.15-1.5	5.4	11.2	711.5	2.78	720.5	2.81	1.26	2.74	498.3
4	17	3.0-4.5	5.4	11.2	726.0	2.83	733.0	2.86	0.96	2.79	498.3
5	7	0.2-1.5	5.4	11.2	732.5	2.86	740.5	2.89	1.09	2.82	724.8
5	19	3.0-4.5	5.4	11.2	724.5	2.83	731.0	2.85	0.90	2.79	447.48
6	4	0.15-1.5	5.4	11.2	722.5	2.82	736.0	2.87	1.87	2.78	362.42
6	20	3.0-4.0	5.4	11.3	709.5	2.74	721.0	2.79	1.62	2.63	447.48
7	9	0.9-1.5	5.4	11.1	702.0	2.76	712.0	2.80	1.42	2.70	407.72
7	24	2.5-4.0	5.4	11.1	611.0	2.40	628.0	2.47	2.78	2.35	181.21
8	6	0.8-2.0	5.4	11.1	609.0	2.40	636.0	2.50	4.43	2.34	135.92
8	18	3.5-4.0	5.4	11.2	632.0	2.47	665.0	2.59	5.22	2.43	135.92
9	5	1.5-2.5	5.3	7.4	391.0	2.40	412.0	2.52	5.37	2.37	88.68
9	15	2.5-4.0	5.4	11.2	687.0	2.68	699.0	2.73	1.75	2.64	271.8
9	23	4.5-5.0	5.4	11.2	720.0	2.81	728.0	2.84	1.11	2.78	200.4
10	12	2.0-3.25	5.4	11.2	674.0	2.63	691.5	2.70	2.60	2.59	407.72
10	14	2.0-3.25	5.4	7.4	378.0	2.23	386.0	2.28	2.12	2.45	40.08
10	17	3.5-5.0	5.4	11.3	563.0	2.18	617.5	2.39	7.90	2.16	45.29
11	4	2.0-3.0	5.5	9.0	526.5	2.46	545.5	2.55	3.61	2.39	71.46
11	20	4.5-5.0	5.5	9.7	498.0	2.16	506.0	2.20	1.61	2.42	107.32
11	12	3.0-4.5	5.4	11.2	578.0	2.25	604.0	2.36	4.50	2.18	135.92
12	8	1.0-2.5	5.4	9.0	488.5	2.37	504.0	2.45	3.17	2.33	75.49
12	11	1.0-2.5	5.4	10.6	525.5	2.17	536.0	2.21	2.00	2.12	111.33
12	16	2.5-4.0	5.4	10.3	554.0	2.35	583.0	2.47	5.23	2.31	87.03
13	16	1.5-3.0	5.4	11.2	708.5	2.76	717.0	2.80	1.20	2.72	543.59
13	7	0.0-0.8	5.4	11.2	618.5	2.41	624.0	2.43	0.89	2.36	187.04
13	25	3.0-4.0	5.4	11.2	610.0	2.38	637.0	2.48	4.43	2.35	90.58
14	4	2.0-3.0	5.3	7.8	383.5	2.23	409	2.38	6.65	2.19	34.6
14	19	3.0-4.0	5.4	5.7	291.0	2.23	309	2.37	6.19	2.22	116.6
14	22	4.0-5.0	5.4	11.2	653.5	2.55	668	2.61	2.22	2.51	447.48
15	9	1.0-2.0	5.4	9.4	540.5	2.51	558	2.59	3.24	2.46	39.42
15	14	2.6-3.5	5.4	11.1	672.0	2.64	689	2.71	2.53	2.58	181.21
15	29	3.5-5.0	5.4	11.1	605.0	2.38	633.5	2.49	4.71	2.32	135.92
16	5	0.25-1.0	5.3	8.1	455.5	2.55	462	2.59	1.43	2.53	486.14
16	41	3.0-4.5	5.4	11.1	605.0	2.38	636	2.5	5.12	2.33	90.58
16	51	4.5-5.0	5.4	11.2	590.0	2.30	618.5	2.41	4.83	2.27	90.58
17	7	1.0-2.5	5.4	11.2	711.5	2.78	719	2.8	1.05	2.68	860.72
17	21	2.5-4.0	5.4	11.2	627.0	2.45	651	2.54	3.83	2.41	181.21
17	25	4.0-5.0	5.4	11.1	628.5	2.47	647	2.55	2.94	2.42	181.21

Chemical Analysis of Soil & Water

Chemical test was conducted to determine the sulphate (SO_4) content, chloride (Cl) content and pH on selected number of disturbed soil sample and water collected from borehole. Results (Table 7) indicated that the values are within limit, hence no special treatment is required.

Engineering Properties

Engineering analysis of the subsoil was performed to determine net safe bearing capacity. Parameters obtained are based on various field and laboratory tests. Rock is encountered at shallow depth. It is considered that isolated pad foundation shall be used. Open foundation - Reference to IS 12070 "Design and construction of shallow foundation on rocks" and IS 13365 (part I) "Quantitative classification system of rock mass". RMR (rock mass rating) of the stratum at foundation depth is determined.

Water loss was noticed in few boreholes. Safe Bearing Capacity was calculated using six parameters for BH-1 for 1m and 2m depth. The value and rating are given in table 8.

Net safe bearing capacity was adopted for pad foundations calculated using above parameters placed at different depth below the ground surface at the time of investigation (Table 9). For foundations placed on rock, it was ensured that there are no loose pockets on rock surface. In

Table 6. Summary of soil test results

BH No.	Depth below GL	Moisture content	Mechanical Analysis		
	(m)	%	% G	% S	% F
9	1.00	2.34	97.0	3.0	0.00
10	1.00	3.65	87.0	9.0	4.00
12	0.75	9.6	83.0	14.0	3.00

Table 7. Chemical analysis of soil and water

S. No.	Location / Depth	SO_4 (mg/kg)	Cl (mg/kg)	pH
1	BH2*	15.47	18.65	7.80
2	BH-5	12.42	20.71	7.36
3	BH-8 /.5m	10.70	12.21	8.05
4	BH-9 /1m	11.24	16.88	7.59
5	BH-11 / 1m	15.65	13.78	7.42
6	BH-16	10.2	12.68	7.89

*Water sample

Table 8. Parameters for calculating safe bearing capacity from BH-1 at depth1&2m

Parameter	Value	Rating
Depth – 1m		
Strength of intact rock (MPa)	59-68%	7
Rock quality Designation	77- 96%	17
Spacing of discontinuities	Wide to very wide	17
Conditions of discontinuities (< 1 mm)	-	23
Ground water condition	Wet	7
Adjustment for joint orientation	Fair	-7
Total		64
Depth – 2m		
Strength of intact rock (MPa)	68	7
Rock quality Designation	91- 96%	20
Spacing of discontinuities	very wide	20
Conditions of discontinuities (< 1 mm)	-	25
Ground water condition	Wet	7
Adjustment for joint orientation	Fair	-7
Total		72

According to IS 12070 (table 3) classification of rock is II

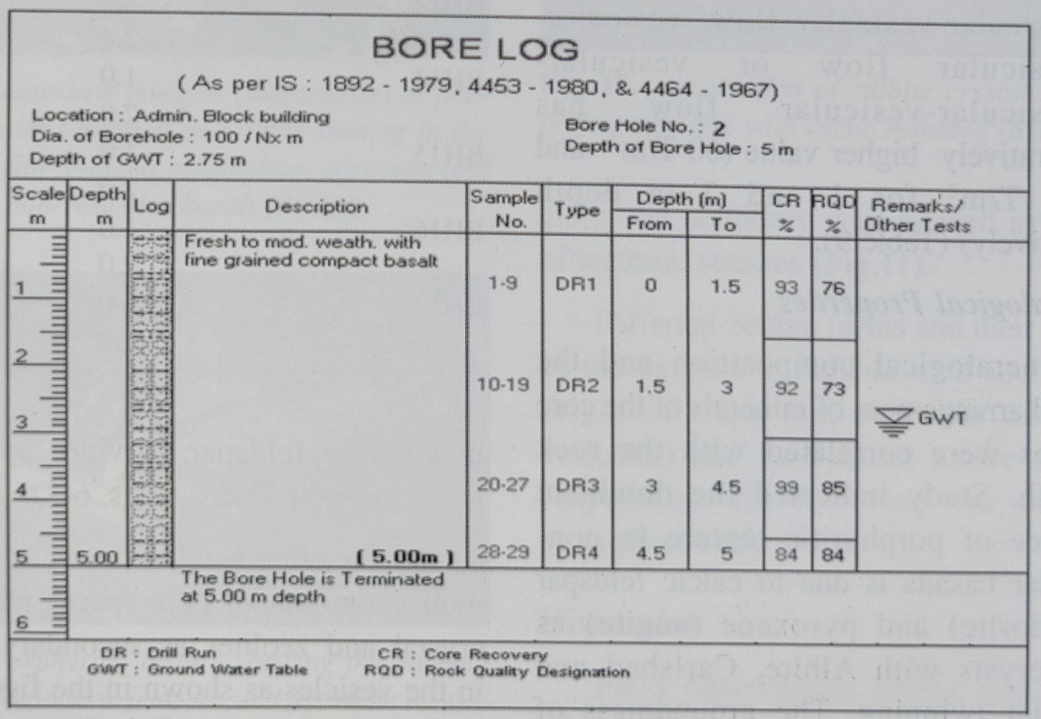

Fig. 5. *Bore log characteristics indicating %RQD and %CR of layer I - IV with depth in non-vesicular flow of Bore Hole No. 2*

case of loose pockets or over excavation, it was filled by plain cement concrete. For foundations placed on gravelly silty sand (muram), prior to placement of PCC, compact bottom of excavation to 95% was filled up with modified proctor density using heavy vibratory roller.

The contour height of the bore hole shows a considerable gap of 9m with variable flow and rock composition which is apparent from the table 3. Study on net safe bearing capacity of different bore holes for the foundation indicated that bore holes with rocks dominant of vesicular flow has very low value (35-45 T/m^2 and 45-55 T/m^2 for 1 and 2 m depth respectively) whereas, bore holes with rocks dominant of nonvesicular flow and or association of nonvesicular-vesicular flow, vesicular-nonvesicular flow or vesicular-nonvesicular-vesicular flow has comparatively higher value (60 T/m^2 and 75-80 T/m^2 for 1 and 2 m depth respectively) (Table 9).

Table 9. Net safe bearing capacity for different bore holes

Borehole No	Depth of foundation (m)	Net safe bearing capacity (T/m^2)
BH1, BH2, BH3, BH4, BH5	1.0	60
	2.0	80
BH6, BH7	1.0	60
	2.5	75
BH8	1.0	60
	2.0	75
BH9	1.0	30
	2.0	50
BH10	1.0	40
	2.0	50
BH11	1.0	35
	2.0	50
BH12	1.5	60
	2.0	80
BH13	1.0	60
	2.0	80
BH14	1.0	45
	2.0	55
BH15	1.0	60
	2.0	80
BH16	1.0	35
	2.0	45
BH17	1.0	60
	2.0	100

Mineralogical Properties

Mineralogical composition and the textural arrangement of minerals of the core samples were correlated with the rock strength. Study indicated the dominant presence of porphyritic texture in non-vesicular basalts is due to calcic feldspar (labradorite) and pyroxene (augite) as phenocrysts with Albite, Carlsbad and Lamellar twinning. The groundmass of theses basalts are mostly dominated by the fine-grained minerals consisting of plagioclase feldspar, olivine, pyroxenes, glass and iron oxides (Figs. 6-8).

On the other hand vesicular basalt have more intergranular pore spaces with larger crystal and zeolites as secondary mineral in the vesicles as shown in the figures 2, 9 and 10, and most of these zeolites are showing dissolution and etching effects

Fig. 6. *Plagioclase feldspar (labradorite) with albite twining in the matrix of pyroxene and olivine in non-vesicular basalt (BH2/8)*

Fig. 7. *Plagioclase feldspar (labradorite) as phenocrysts with Carlsbad and albite twining in the matrix of fine grained plagioclase, pyroxene and olivine in non-vesicular basalt (BH2/8)*

Fig. 8. *Porphyritic texture showing the phenocrysts of plagioclase feldspar and pyroxene as well in the groundmass of non-vesicular basalt. (BH2/8)*

Fig. 9. *Plagioclase feldspar (labradorite) in the matrix of altered pyroxene and olivine in vesicular basalt(BH 10/9)*

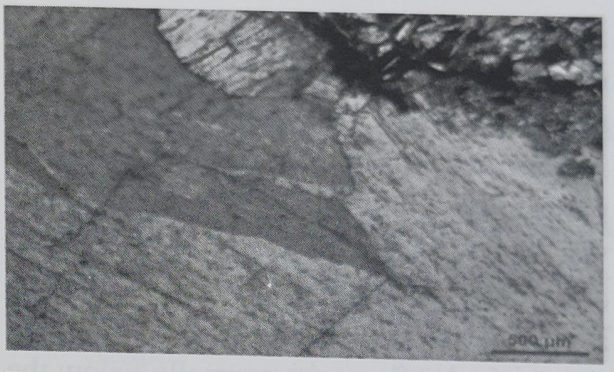

Fig. 10. *Association of stilbite crystal showing perfect cleavage with cyclic twinning (BH8/2)*

along the boundary wall as well as effects of tectonic stresses (Fig.11).

Different zeolite forms and their growth in the cavities is indicative of multifacets origin of traps (i.e. vesicular and non-vesicular) and its hydrous nature may be responsible for lowering the shearing strength of rock.

Discussion

Field observations shows two phases of volcanic activity/magmatic eruption which are indicated by vesicular

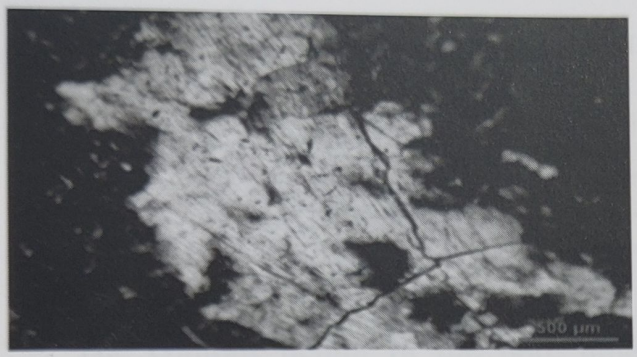

Fig. 11. *Stilbite minerals are showing dissolution and etching effects along the boundary wall as well as effects of tectonic stress (BH 8/23)*

(amygdular), non-vesicular (ordinary) and combination of these flows that occurred in the area during the Upper Cretaceous period (68.5 million years). Due to low viscosity of magmatic fluids, vesicular flow are widely distributed on the ground, vis-à-vis higher viscous magmatic fluids of non-vesicular flow are normally below the ground and are exposed in the area whereas the upper horizon of vesicular flows has been removed / eroded due different weathering agencies.

Results on geotechnical analysis indicated most variable physical parameters are the saturated crushing strength followed by the water absorption. The reasons for this variation are due to the inhomogeneous and fractured / altered nature of rocks in different horizons and at variable depths at logging site. Based on the RMR, IS 12070 recommended safe bearing capacity value. According to IS 12070, allowable pressure will result (in raft up to 6 m thickness) in settlement less than 12 mm. In some of the boreholes higher bearing capacity is possible, lower value is recommended due to presence of alternate layers with low RQD.

Results on mineralogical associations with different rock units shows that due to presence of more intergranular pore spaces (amygdales/cavity) with larger crystal of feldspars and secondary dissoluted zeolites the rock strength is lowered which lowers the net safe bearing capacity therefore foundation will be weak. Contrary to this, in the non-vesicular flow the intergranular pore spaces between mineral grains of feldspars, olivine and pyroxenes as well as zeolites are highly compact and therefore rock strength is high resulting higher net safe bearing capacity and therefore foundation will be strong. This indicates that due to varying flow with diverse lithology the different treatment for the foundations are required to set up a strong base of different blocks.

Conclusions

The high net safe bearing capacity and shearing strength of non-vesicular basalt is due to compactness of rock with least weathered fine grained primary silicate minerals and lower net safe bearing capacity of vesicular basalt is due to presence of coarse mineral grains with larger intergranular pore spaces and weathered mineral grains.

Acknowledgements

Author is thankful to the Director, NIASM, Baramati for providing the facility and Soil Tech (India) Pvt. Ltd., Pune for analyzing engineering parameters.

References

Coduto, *et al.* Donald 2011. *Geotechnical Engineering Principles and Practices*. New Jersey: Pearson Higher Education. ISBN 9780132368681

Duraiswami, R.A. 2009. Pulsed inflation in the hummocky lava flow near Morgaon, Western Deccan Volcanic Province and its significance. *Current Science.* **97**: 313-316

Kanegaonkar, N.B. and Powar, K.B. 1978. Genesis of Plagioclase megacrysts in porphyritic basalts of Purandhar hills, Western Maharashtra. Recent Res. Geol., Hindustan Publ. Corp, Delhi., **4**: 313-332.

Kale, V.S. and Rajaguru, S.N. 1987. Late Quaternary alluvial history of the northwestern Deccan Upland Region. *Nature.* **325**: 612-614.

Kale, V.S., Patil, D.N., Pawar, N.J., Rajaguru, S.N. 1993. Discovery of volcanic ash bed in the alluvial sediments at Morgaon, Maharashtra. *Man and Environment.* **18** : 141-143.

Godbole, S. M., Rana, R. S., Natu, S. R. 1996. Lava stratigraphy of Deccan basalts of western Maharashtra. Gondwana Geol. *Mag. Spl. Publ.* **2**: 125-134.

Geological Survey of India 1998. Quadrangle Geological Map of Baramati Quadrangle. Government of India Press.

Read, H.H. 1963. Rutley's Elements of Mineralogy. Twenty Fifth Edition, Thomas Murbay Publication, London, 525pp.

Kar, P.F. 1977. Optical Mineralogy. Mcgraw Hill, 442 pp.

Terzaghi, K., Peck, R.B. and Mesri, G. 1996. *Soil Mechanics in Engineering Practice* 3rd Ed., John Wiley & Sons, Inc. ISBN 0-471-08658-4.

(Received October 2014; Accepted April, 2015)

Clay Research, Vol. 33, No. 2, pp. 110-125 (2014)

Weathering of Silicate Minerals by Humic Acids : III. Nature of Cation Solubilisation from Epidote and Microcline and Characteristics of the Residual Products

SRUTI DAS, KUNAL GHOSH AND CHANDRIKA VARADACHARI

Raman Centre for Applied and Interdisciplinary Sciences, 16A Jheel Road, Kolkata 700 075

Abstract–*This study aims to understand the alteration of the primary minerals, epidote (sorosilicate) and microcline (tectosilicate) by humic acids (HAs) of diverse origin (extracted from Entisol, Alfisol and Mollisol). Kinetics of dissolution as well as nature of residues formed after weathering, were investigated. The solubilisation process represents a cycle of alternate dissolution and precipitation as seen from the recurring crests and troughs in the kinetic curves. The release of cations from the minerals is determined by its position in the crystal lattice, its strength of chelation with HA, accessibility of HA to the ion and the how the neighbouring ions are affected by its removal. Analysis of the residual products further illustrates the contrasting stabilities of the minerals. The composition of epidote showed significant reduction in* Si^{4+}, $Fe^{2+/3+}$ *and* Ca^{2+} *and enrichment in* Al^{3+} *with all the HAs; microcline showed only slight reduction in* Si^{4+}, $Fe^{2+/3+}$ *and* K^{+} *and enrichment in* Al^{3+}. *The major XRD bands of microcline were unchanged in the residues and no new phases were observed. Epidote residue showed significant changes in many XRD bands and the formation of new phases. The IR spectra of both the minerals showed absorptions due to HA indicating the precipitation of metal-HA complex on mineral surface.*

Key words : Weathering, silicates, epidote, microcline, humic acids, cation, solubilisation.

Of the six groups of primary silicate minerals, two earlier publications (Das *et al.*, 2013, 2014) described the weathering of olivine (nesosilicate), tourmaline (cyclosilicate), hornblende (inosilicate) and biotite (phyllosilicate) by humic acids (HAs) particularly the nature of cation solubilisation and characteristics of the residual products. Here, we are extending such studies to the remaining two groups, viz., epidote (sorosilicate) and microcline (tectosilicate).

The kinetics of reactions involving solid phases in solutions is complex due to formation of surface coats, etching and fragmentation. Studies on silicate dissolution by organic acids have been mostly confined to simple organic acids;

***Corresponding Author Email :** kghoshcu@gmail.com

humic acid dissolutions of silicates have been rather limited. In studies of organic acid dissolution of primary silicates, Barman *et al.* (1992) concluded that organic acids dissolved minerals by a combined action of complexation and acid attack. The solubilities of the cations depend on their positions within the crystal. At the initial stages, the rate determining step was surface detachment of cation-ligand complexes. Subsequently, the creation of fresh surfaces by fragmentation and etching were rate-limiting (Barman *et al.*, 1992). Olivine and biotite showed fragmentation to small particles whereas microcline and tourmaline showed dissolution of ultrafine particles (Varadachari *et al.*, 1994). Biotite also had reduction in size of flakes, tearing of edges and reduction in thickness of the layers.

Earlier workers studying mineral dissolution had inferred that mechanism of dissolution proceeds by a surface-controlled reaction (Hansley and Briggs, 1994). Organic acids significantly enhance feldspar dissolution rates (Hees *et al.*, 2000 ; Welch and Ullman, 1996). The organic promoted dissolution of silicates increased at moderately acidic to near neutral pH (Knauss and Copenhaven, 1995). Organic dissolution, whichwas roughly pH independent (Wogelius and Walther, 1992), was weak and enhanced only in neutral pH (Golubev and Pokrovsky, 2006). However, Drever (1997) found that HAs do not increase feldspar dissolution rates significantly. Organic acids can directly enhance dissolution by proton/ligand-mediated mechanism (Furrer and Sticher, 1999) with rate being proportional to the concentration of adsorbed ligand or indirectly by complex formation with reaction products (Bennett, 1991) thereby increasing the chemical affinity for dissolution. The adsorption of ligands in feldspar occurs primarily at Al sites on the surface (Welch and Ullman, 1996) forming Al-organic complexes (Wit *et al.*, 2001) and this weakens the Al-O bonds of feldspar, resulting in leaching Al into solution and enriching the surface with strongly bonded Si-OH in place of the weakly bonded Al-OH (Drever, 1997).

A series of studies on weathering of various primary silicate minerals by HAs was conducted by Das *et al.* (2013, 2014). These two previous investigations reported the changes to olivine, tourmaline, hornblende and biotite covering the mineral groups belonging to the nesosilicate, cyclosilicate, inosilicate and phyllosilicate. Das *et al.* (2013) observed that weathering of minerals by HAs showed marked differences from weathering by low molecular weight organic acids. Dissolution did not show a regular increase but a series of peaks and troughs indicating precipitation (Das *et al.*, 2013). There were significant alterations in crystallinity as seen from XRD. Similar kinetic patterns of peaks and troughs were also observed with hornblende and biotite dissolution by HAs (Das *et al.*, 2014). XRD bands of biotite

were minimally altered whereas major XRD bands of hornblende either disappeared from the diffractogram or were much reduced in intensity (Das *et al.*, 2014).

This work, which is an extension of the two previous investigations by Das *et al.* (2013, 2014), completes the study of the weathering of the major silicate groups.; The sorosilicates and tectosilicates represented by epidote and microcline were weathered by HAs obtained from diverse agro-climatic origins. Investigations on the kinetics of dissolution of cations from epidote and microcline by HAs extracted from an Entisol, Alfisol and Mollisol were carried out at varying pH. The residual products of the reactions were studied for compositional changes and also changes in their XRD and IR spectra.

Materials and Methods

Characterisation of minerals

Epidote (sorosilicate) and microcline (tectosilicate) provided by the Geological Survey of India, Kolkata were used in this study. The minerals were powdered and dry-sieved to the 80-150 mesh B.S. size fraction, then washed and dried at 80°C. X-ray diffraction (XRD), infrared spectroscopy (IR) and chemical analysis of the minerals and their weathered products were done as described by Das *et al.* (2013, 2014).

Extraction and characterisation of humic acids

The HAs were extracted from surface soils (0-15 cm) of an Entisol (Fine loamy, mixed, hyperthermic, Aeric Fluvaquent; deltaic new alluvium; Baruipur, W. Bengal), Alfisol (Fine loamy, kaolinitic, hyperthermic, Ultic Paleustalf; ferruginous soil; Vishnupur, W. Bengal) and Mollisol (Coarse loamy, mixed, cryic, Typic Hapludoll; mountain soil; Auli, Uttarakhand). The method of extraction, fractionation, purification and characterisation of HAs was carried out as described by Das *et al.* (2013).

Elimination of interference by humic acids in the chemical analysis of cations

Spectrophotometric methods for the determination of cations in solution in the presence of HA had to be slightly modified because HA interferes in colour development procedures. Modifications adopted herein were described by Das *et al.* (2013).

Kinetics studies

Kinetics of solubilisation of cations from the minerals by HAs were studied in the following the procedure described in earlier studies (Das *et al.*, 2013, 2014). To 200 mg of mineral sample in plastic bottles, 20 ml of 1000 ppm HA was pipetted in. The pH of HA was varied from 6-9. The suspensions were shaken intermittently (8h/day) up to 49 days. At the end of the reaction period, which was 7, 14, 21, 28, 35, 42 and 49 days, the solutions were

filtered, washed, made to volume and analyzed for the major cations.

Studies on residual products

Weathered products of reaction were prepared as followed in earlier studies (Das *et al.*, 2013, 2014). To 2 g mineral sample in a plastic bottle, 50 ml of 1000 ppm HA was added and the solutions agitated on a shaker intermittently (5h/day) for three consecutive months. The residues were then filtered, washed and dried in an oven at 80°C. These were analyzed for the major cations as described for untreated minerals.

Results and Discussion

The mineral epidote belongs to the epidote group of the epidote series and the feldspar is a microcline (Tables 1 and 4) (Deer *et al.*, 1985).

Elemental analysis data of the humic acids on dry ash-free basis were 55.20% C, 5.05% H, 4.36% N and 35.39% O for Entisol HA, 54.90% C, 6.51% H, 5.64% N and 32.95% O for Alfisol HA, 57.47 % C, 5.91% H, 4.83% N and 31.79% O for Mollisol HA (Das *et al.*, 2013, 2014). The E_4/E_6 ratios of the HA samples were 4.29, 3.27 and 4.23 for Entisol, Alfisol and Mollisol Has, respectively (Das *et al.*, 2013, 2014), suggesting that aromacity (Kononova, 1966) or particle size (Ghosh and Schnitzer, 1979) follows the order like Alfisol HA > Mollisol HA > Entisol HA. The NaOH titratable acidity values were 2.50, 2.60 and 3.50 meq/g and total acidities were 5.90, 6.66 and 8.50 meq/g for Entisol, Alfisol and Mollisol Has, respectively (Das *et al.*, 2013, 2014). IR spectra of the humic acids show absorptions at 3750, 3400, 2900 2370, 1600, 1200, 1000, 660 cm^{-1} (Das *et al.*, 2013).

Table 1. *Chemical composition of the silicate minerals*

% Oxide	Epidote	Microcline
SiO_2	44.46	71.25
$FeO+Fe_2O_3$	11.11	0.11
Al_2O_3	21.79	16.83
TiO_2	0.57	N.D.
CaO	21.30	N.D.
MgO	1.54	N.D.
Na_2O	N.D.	0.66
K_2O	N.D.	11.32
H_2O^-	0.02	N.D.
H_2O^+	0.79	N.D.

Order of cation solubilisation from the minerals

Cation release from epidote and microcline (Fig. 1) shows alternate cycles of rise and fall with all HAs at all pH. This cyclic pattern has been attributed to solubilisation and precipitation after complexation with HA (Das *et al.*, 2013, 2014). Variation in pH has little effect on cation solubilisation.

The order of release of cations from epidote shows that $Fe^{2+/3+}$ is most solubilised (Figs. 1) and is followed by Al^{3+}; Ca^{2+} and Si^{4+} are least solublised with both Entisol and Mollisol HAs. Alfisol HA solubilises more Ca^{2+} compared to Al^{3+}, the order of release being $Fe^{2+/3+} > Ca^{2+} \geq Al^{3+} > Si^{4+}$.

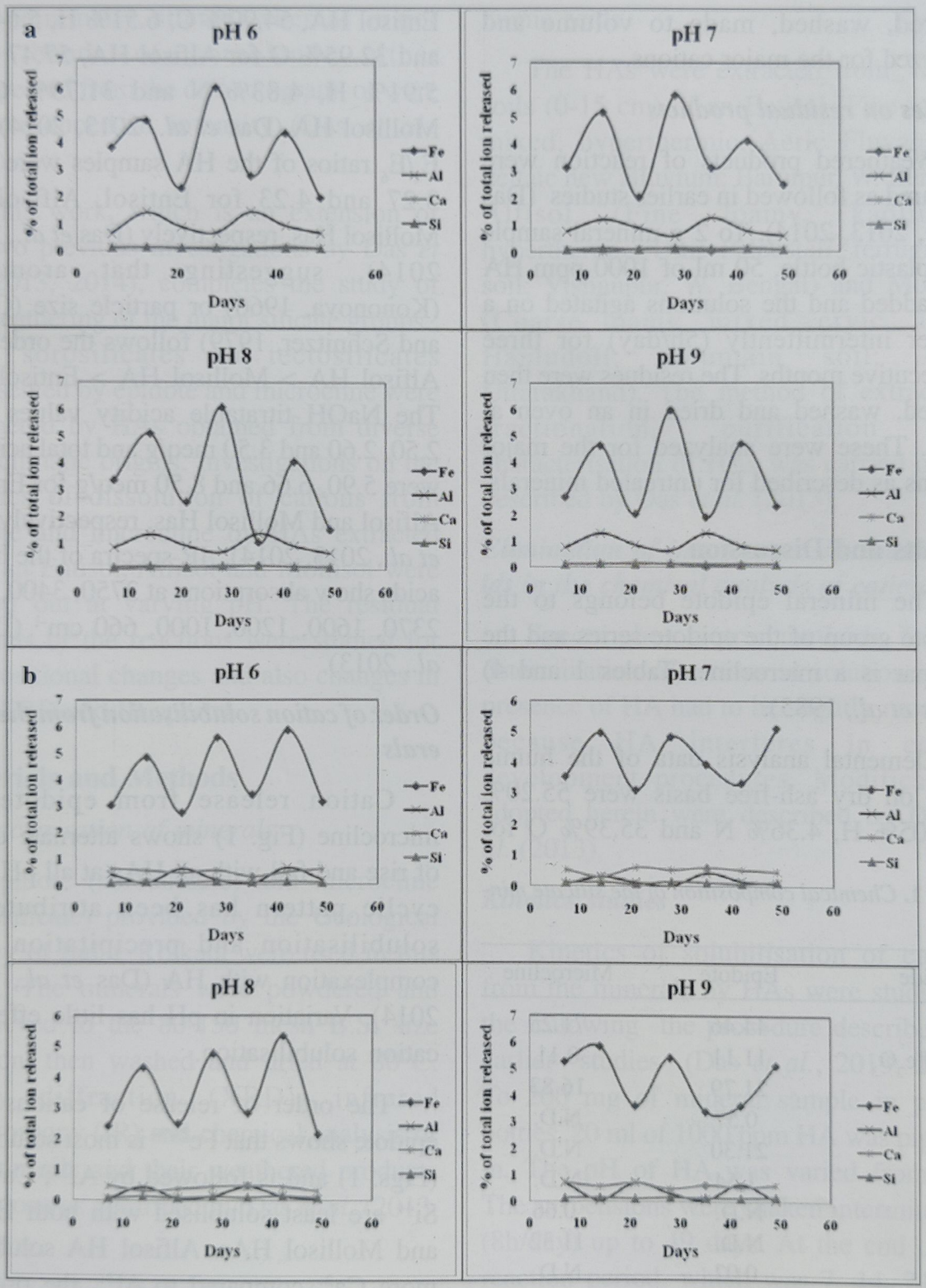

Fig. 1. (A) *Release of cations from (a) Epidote by Entisol HA and (b) Epidote by Alfisol HA*

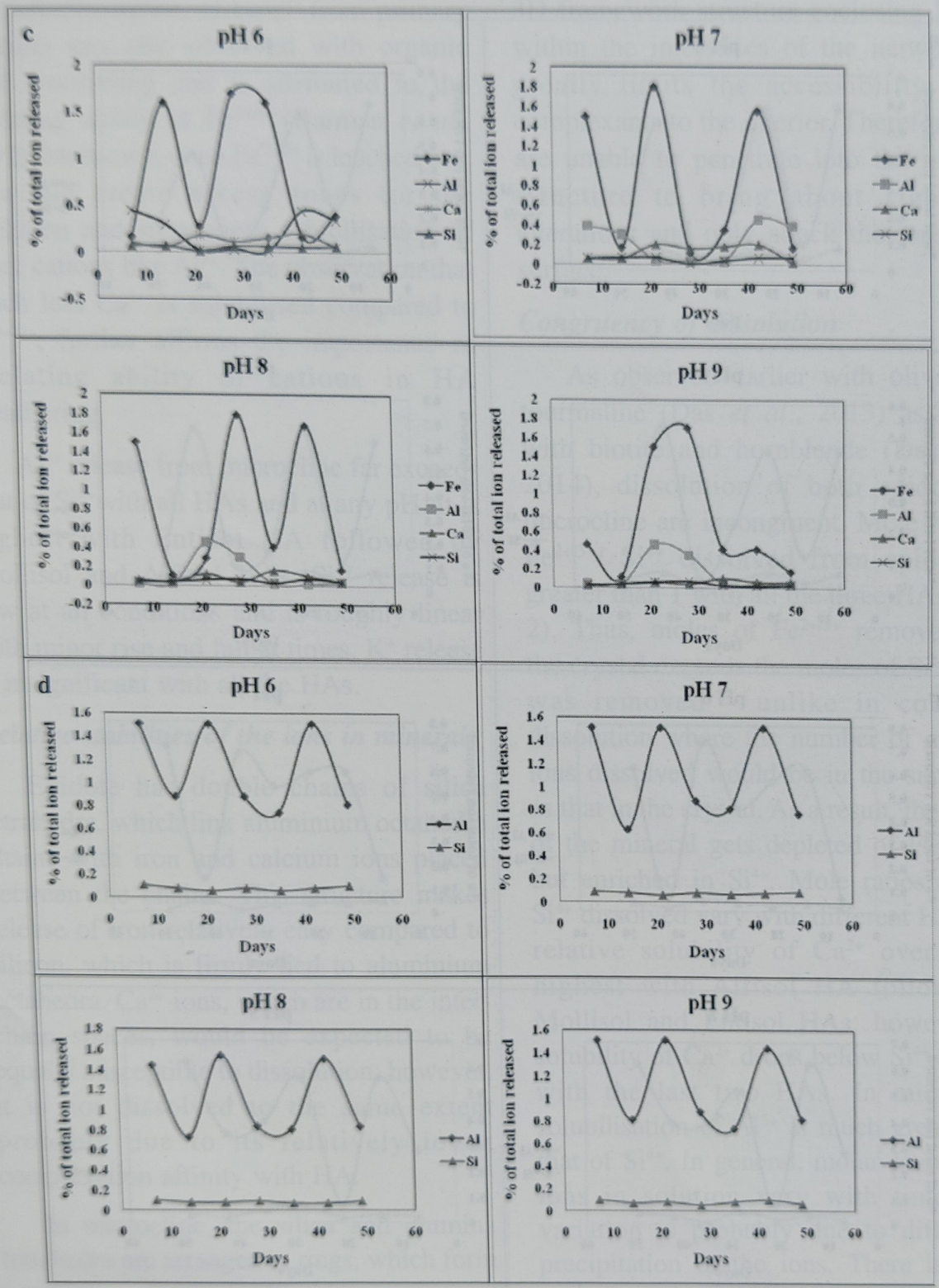

Fig. 1. (B) *Release of cations from (c) Epidote by Mollisol HA and (d) Microcline by Entisol HA*

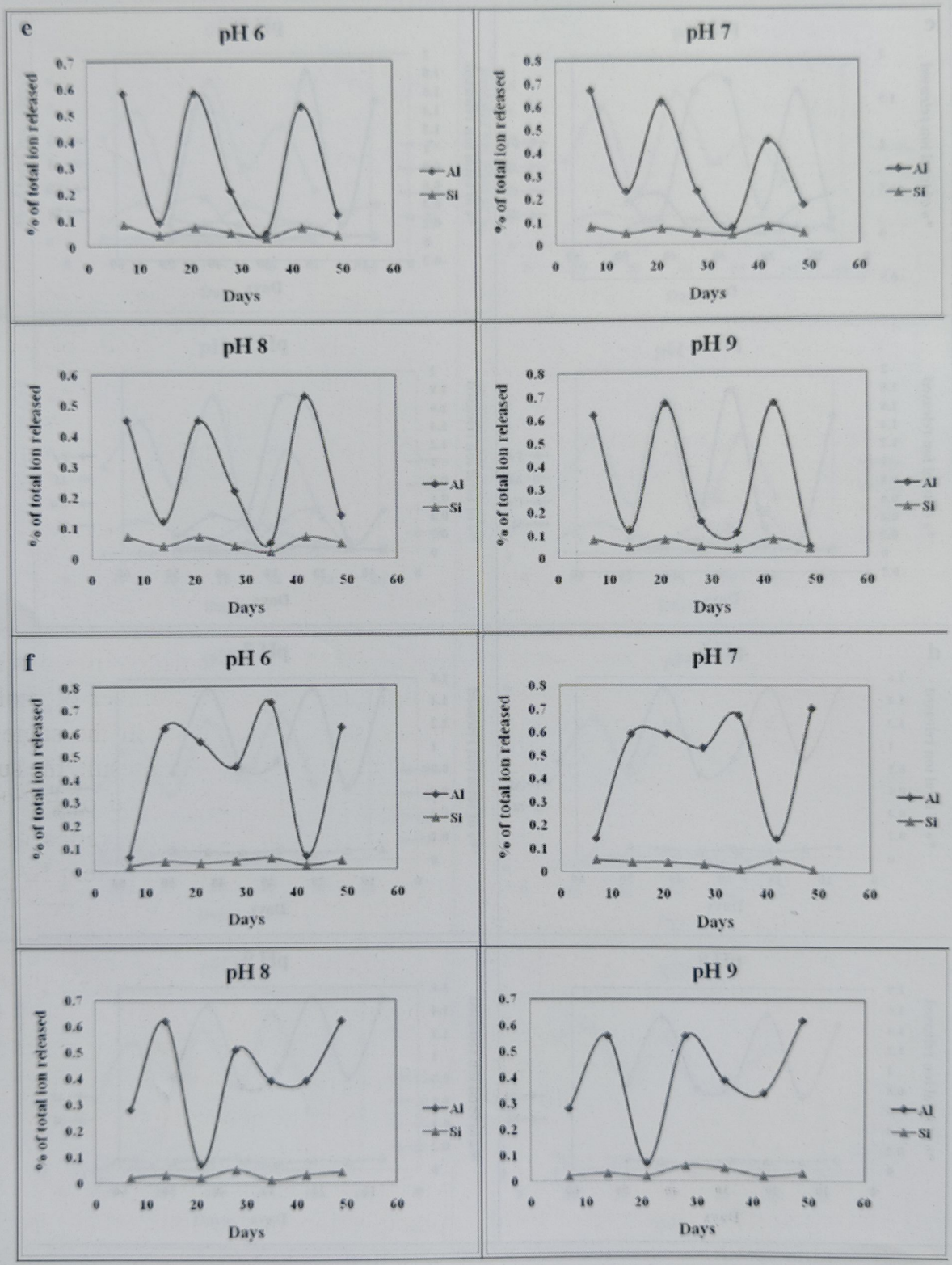

Fig. 1. (C) *Release of cations from (e) Microcline by Alfisol HA and (f) Microcline by Mollisol HA*

Highest dissolution of $Fe^{2+/3+}$ from primary silicates was also observed with organic acid weathering and is attributed to the chelating ability of $Fe^{2+/3+}$ (Barman *et al.*, 1992). Moreover, once $Fe^{2+/3+}$ is leached out, it would create access zones for the chelation and subsequent solubilisation of other cations like Al^{3+}. The observation that much less Ca^{2+} is solubilised compared to $Fe^{3+/2+}$, further affirms the importance of chelating ability of cations in HA weathering.

Al^{3+} release from microcline far exceeds that of $Si^{4+}$with all HAs and at any pH. It is highest with Entisol HA followed by Mollisol and Alfisol HAs. Si^{4+} release is low at all conditions and is roughly linear with minor rise and fall at times. K^{+} release is insignificant with all the HAs.

Relative stabilities of the ions in minerals

Epidote has double chains of silica tetrahedra, which link aluminium octahedra chains with iron and calcium ions placed between the chains. This structure makes release of iron relatively easy compared to silicon, which is firmly tied to aluminium octahedra. Ca^{2+} ions, which are in the inter-chain spaces, would be expected to be equally susceptible to dissolution; however, it is not dissolved to the same extent probably due to its relatively lower complexation affinity with HA.

In microcline, the silica and alumina tetrahedra are arranged in rings, which form continuous chains resulting into a compact 3D framework structure enclosing K^{+} ions within the interstices of the network that greatly limits the accessibility of the complexants to the interior. Therefore, HAs are unable to penetrate into this intricate structure to bring about significant alterations and only attack the ions at the surface.

Congruency of dissolution

As observed earlier with olivine and tourmaline (Das *et al.*, 2013) as well as with biotite and hornblende (Das *et al.*, 2014), dissolution of both epidote and microcline are incongruent. Mole ratios of $Fe^{2+/3+}$/ Si^{4+} dissolved from epidote are greater than 1 with all the three HAs (Table 2). Thus, moles of $Fe^{2+/3+}$ removed from the crystal exceeds the moles of Si^{4+} which was removed – unlike in congruent dissolution where the number of moles of ions dissolved would be in the same ratio as that in the crystal. As a result, the surface of the mineral gets depleted of $Fe^{2+/3+}$ and but enriched in Si^{4+}. Mole ratios of Al^{3+}/ Si^{4+} dissolved vary with different HAs. The relative solubility of Ca^{2+} over Si^{4+} is highest with Alfisol HA followed by Mollisol and Entisol HAs; however, the solubility of Ca^{2+} drops below Si^{4+} at times with the last two HAs. In microcline, solubilisation of Al^{3+} is much greater than that of Si^{4+}. In general, molar ratios of the ions in solution vary with time. Such variation is probably due to differential precipitation of the ions. There is also a variation with pH, which could be due to

Table 2. *Mole ratio of cations/ Si^{4+} solubilised from minerals by various HAs*

Mole ratio	HA	pH	Epidote							Microcline						
			Days							Days						
			7	14	21	28	35	42	49	7	14	21	28	35	42	49
$Fe^{2+/3+}/Si^{4+}$	Entisol	6	30.32	31.62	17.68	42.93	26.22	33.05	18.17							
		7	32.59	35.66	18.78	38.76	24.07	31.62	29.64							
		8	29.67	32.55	23.60	36.06	10.86	31.19	14.21							
		9	22.21	29.37	15.38	37.48	15.83	36.08	19.31							
	Alfisol	6	31.85	36.97	32.97	39.27	32.06	42.65	33.91							
		7	29.70	35.86	33.19	31.44	30.06	33.60	34.26							
		8	26.87	31.48	26.45	33.66	25.58	34.25	22.83				Nil			
		9	44.90	42.70	36.56	36.06	25.76	14.77	33.66							
	Mollisol	6	2.62	22.44	12.02	26.23	22.44	2.89	6.12							
		7	24.90	2.40	27.11	19.25	8.25	21.58	2.62							
		8	34.58	3.21	4.81	24.85	13.46	25.35	4.51							
		9	15.27	3.01	24.90	26.23	13.45	22.44	5.77							
Al^{3+}/ Si^{4+}	Entisol	6	5.19	9.46	6.89	4.86	13.87	7.30	6.26	14.30	11.65	23.93	10.59	12.88	19.33	8.28
		7	8.13	8.42	8.30	4.02	9.84	6.00	7.14	16.75	8.38	25.12	11.65	11.96	18.61	8.74
		8	7.40	8.49	8.46	4.02	14.17	6.89	5.91	14.07	8.67	20.38	9.04	11.96	20.10	9.34
		9	6.33	8.33	6.69	4.09	10.88	6.29	5.42	15.95	11.96	18.61	16.18	9.71	14.71	13.45
	Alfisol	6	4.24	0.62	7.27	1.23	0.52	4.66	1.89	7.69	2.33	8.75	4.44	1.68	7.80	2.83
		7	0.67	2.14	1.36	0.25	3.22	1.76	0.63	8.15	4.79	8.56	4.26	1.80	5.98	3.40
		8	0.62	3.21	0.86	0.90	4.06	0.82	0.59	6.10	3.29	6.64	5.53	2.24	7.32	3.11
		9	5.8	0.31	6.88	1.97	0.50	2.59	0.25	7.75	2.74	8.97	2.99	2.54	8.79	1.35
	Mollisol	6	6.89	4.15	0.83	0.66	0.28	7.58	5.25	2.49	16.44	18.68	11.95	16.18	3.73	16.44
		7	6.47	4.15	0.66	4.32	0.62	6.36	5.89	2.87	15.69	15.69	17.75	8.97	3.11	9.34
		8	0.46	0.55	7.64	4.15	0.66	0.30	0.67	18.69	20.55	3.74	10.35	5.23	13.08	16.44
		9	1.44	0.67	7.60	5.25	1.44	1.44	0.86	18.69	18.68	3.74	9.96	8.72	14.95	18.27
Ca^{2+}/ Si^{4+}	Entisol	6	1.02	1.05	0.98	0.69	1.21	1.48	1.18							
		7	0.99	0.22	1.18	0.64	0.25	0.98	1.14							
		8	0.28	0.61	1.18	0.57	1.67	0.98	0.91				Nil			
		9	1.07	0.82	1.48	0.80	0.27	0.74	1.07							

Table 2. *Continued*

Mole ratio	HA	pH	Epidote						Microcline					
			Days						Days					
			7	14	21	28	35	42	49	7	14	21	28	35	42	49
	Alfisol	6	6.30	4.10	5.31	3.76	2.95	3.43	6.13							
		7	4.42	2.25	6.33	3.47	4.51	5.37	3.16							
		8	5.24	2.29	3.98	3.10	4.24	2.82	3.32							
		9	5.87	4.12	6.96	3.11	4.51	2.17	3.88							
	Mollisol	6	1.45	0.77	7.30	1.75	2.16	3.25	0.84							
		7	0.93	0.77	2.95	5.89	4.17	2.71	0.24							
		8	1.29	1.00	1.92	0.50	5.17	1.45	0.93							
		9	0.53	0.93	0.93	0.54	3.18	3.10	1.86							

the dual factors of influence of pH on dissolution rate as well as precipitation.

Kinetics of dissolution

The pattern of dissolution of epidote and microcline is different from the known pathways of dissolution of silicates in water, inorganic and low-molecular weight organic acids (Barman *et al.*, 1992). An alternate cycle of peaks and troughs,which may be due to successive dissolution and precipitation, is observed and it is not a usual linear kinetics. The ions are complexed and brought into solution by HA and once it exceeds a critical concentration, precipitation occurs leading to further dissolution. The solubilisation pattern did not change with time or with pH. Chelation seems to be the dominant mechanism of cation release (Schalscha *et al.*, 1967) by HA; specific adsorption on the mineral surfaces (Stumm and Furrer, 1987; Stumm and Wieland, 1990) also plays a part.

Study of residues

Chemical analysis

Epidote residue after weathering by HA, showed substantial changes in chemical composition (Table 3); there was a reduction in Si^{4+}, $Fe^{2+/3+}$ and Ca^{2+} and enrichment in Al^{3+}. The decrease in $Fe^{2+/3+}$ content wass highest with Alfisol HA and Ca^{2+} with both Entisol and Mollisol HA. The reduction in Si^{4+} was largest with both Alfisol and Mollisol HA.

Microcline residue showed only minor

reduction in Si^{4+}, $Fe^{2+/3+}$ and K^{+} contents but a substantial increases in Al^{3+} (Table 3). Alfisol HA caused largest changes.

Both the minerals showed increase in adsorbed water (H_2O^-) as well as structural water (H_2O^+), which may be due to deposition of HA on the mineral surface.

XRD studies

The diffraction patterns of epidote after weathering by HAs weakened considerably (Table 4). The main characteristic band of epidote disappeared and many other diffraction bands either vanished or were much reduced. The strongest band of epidote at 3.15 Å is absent in all the weathered residues; this is also true of the second strongest band at 4.28 Å (Table 3). Instead, the weathered residues show the emergence of new reflections with the strongest band at 2.03 Å. The new reflections suggest the formation of compounds like calcium aluminium silicate hydrate, calcium aluminium silicate, calcium aluminium silicate hydroxide and calcium aluminium carbonate hydroxide hydrate (JCPDS 1980, 1983, 1984; JCPDS, 1987). This indicates that the Ca^{2+} is dissolved and then precipitated in some other forms.

The XRD bands of microcline showed changes (Table 4). The main band of microcline at 3.50 Å was absent in the Entisol and Mollisol HA weathered products. The second strongest band at 3.73 Å was nearly absent in all weathered

Table 3. *Percent change in ionic constituents on weathering*

Humic acid	Mineral		%Si	% change	% Fe	% change	% Al	% change	% Ca	% change	%K	% change	H_2O-	H_2O+
	Epidote	O	20.75		8.63		11.50		15.20		-		0.02	0.79
Entisol		W	19.00	-8.4	7.90	- 8.5	14.50	+26.1	11.25	-32.6	-	-	1.02	3.20
Alfisol		W	18.00	-13.3	6.54	-24.2	16.00	+39.1	12.85	-15.5	-	-	0.95	2.90
Mollisol		W	18.00	-13.3	8.50	-1.5	15.70	+36.5	10.80	-29.0	-	-	0.80	3.20
	Microcline	O	33.25		0.09		8.90		-		9.40		0.01	0.80
Entisol		W	33.00	-0.8	0.07	-23.5	9.00	+15.49	-	-	9.30	-1.1	0.03	1.20
Alfisol		W	32.20	-3.2	0.05	-41.2	10.30	+26.29	-	-	9.00	-4.3	0.02	1.05
Mollisol		W	33.00	- 0.8	0.06	-35.3	9.50	+15.49	-	-	9.20	-2.1	0.05	1.40

O : Original mineral W : Weathered mineral % Change (-) : indicates deposition

Table 4. *XRD data of epidote and microcline and its residues*

Epidote								Microcline							
Original		Weathered by Entisol HA		Weathered by Alfisol HA		Weathered by Mollisol HA		Original		Weathered by Entisol HA		Weathered by Alfisol HA		Weathered by Mollisol HA	
d (A^0)	I	d (A^0)	I	d (A^0)	I	d (A^0)	I	d (A^0)	I	d (A^0)	I	d (A^0)	I	d (A^0)	I
8.53	2	6.16	10	4.06	3	6.18	3	10.13	36	5.9	3	4.25	12	4.29	10
6.77	2	5.79	8	3.24	4	3.54	20	6.56	29	4.26	5	4.0	8	4.02	13
5.08	18	3.6	8	2.68	3	3.48	3	6.0	7	3.83	3	3.86	3	3.89	10
4.57	8	3.26	10	2.61	3	3.25	6	5.39	2	3.75	8	3.51	100	3.82	10
4.28	48	2.35	75	2.52	3	2.63	6	5.04	6	3.4	5	3.39	17	3.7	9
3.51	26	2.18	7	2.46	3	2.45	3	4.63	4	3.27	70	3.25	50	3.73	6
3.35	29	2.03	100	2.33	3	2.34	10	4.25	49	2.97	4	3.21	23	3.4	48
3.27	18	1.81	8	2.29	3	2.16	3	4.01	27	2.78	5	2.93	30	3.28	22
3.15	100	1.78	5	2.17	4	2.09	6	3.95	13	2.65	5	2.9	28	3.23	63
2.95	3	1.63	7	2.06	3	2.03	100	3.86	47	2.58	3	2.63	17	3.0	16
2.82	3			2.03	100	1.87	3	3.79	16	2.53	3	2.57	13	2.91	24
2.61	11			1.96	3	1.81	3	3.73	76	2.48	3	2.53	27	2.8	6
2.54	2			1.88	3	1.75	3	3.68	11	2.35	10	2.44	5	2.52	4
2.46	26			1.79	3	1.66	3	3.61	13	2.24	3	2.4	3	2.45	6
2.4	2			1.65	15			3.5	100	2.03	100	2.35	43	2.36	12
2.34	8							3.39	38	1.98	8	2.3	3	2.24	7
2.23	3							3.26	58	1.81	3	2.25	3	2.18	22
2.17	25							3.2	24	1.74	3	2.17	17	2.17	16
2.05	8							3.14	3	1.62	3	2.03	80	2.04	100
2.03	35							3.04	13			1.93	9	1.99	13
2.01	11							2.96	16			1.87	3	1.97	9
1.91	2							2.9	16			1.8	4	1.88	7
1.89	18							2.8	13			1.74	6	1.82	28
1.83	8							2.76	5			1.71	3	1.74	7
1.8	2							2.7	2			1.66	6		
1.73	6							2.55	4			1.59	3		
1.64	75							2.44	13						
1.56	3							2.4	4						
1.46	20							2.35	13						

Table 4. *Continued...*

Epidote							Microcline						
Original		Weathered by Entisol HA		Weathered by Alfisol HA		Weathered by Mollisol HA	Original		Weathered by Entisol HA		Weathered by Alfisol HA		Weathered by Mollisol HA
d (A^0)	I	d (A^0)	I	d (A^0)	I	d (A^0)	d (A^0)	I	d (A^0)	I	d (A^0)	I	d (A^0)
1.43	9						2.23	4					
1.41	8						2.16	13					
1.28	31						2.09	4					
							2.04	67					
							1.97	9					
							1.93	5					
							1.89	5					
							1.87	11					
							1.8	13					
							1.77	9					
							1.72	4					
							1.66	13					
							1.61	4					

residues. The 3.26 Å band was, however, retained. Overall, the impression gained from XRD is that although there were changes to the crystal structure, yet new crystalline phases are not formed as with epidote. Probably the extent of dissolution was not sufficient to form new phases.

IR spectroscopic studies

The residues formed after treatment of epidote are characterised by the presence of all the bands characteristic of epidote (Farmer and Russel, 1964) as well as those of HAs. Strong vibrations around 1000 cm^{-1} due to $\tilde{o}_{as}$ Si-O-Si are observed along with vibrations around 950, 650 and 520 cm^{-1} (below 1000 cm^{-1}) assigned to $\tilde{o}_s$ Si-O-Si and Si-O_t as well as those due to linking cations in epidote and its weathered products. Vibrations around 720 cm^{-1} and 450 cm^{-1} observed in some of the residues may be attributed to the $\tilde{o}_s$ modes of Si-O-Si and lattice vibrations. Absorptions around 3754, 3360, 2370 cm^{-1} in the spectrum of the weathered residues could also be contributions from OH groups of HA precipitated on the surface of the residue.

Weathered microcline residues also show overlapping of microcline absorptions with those

of HAs. Vibrations around 1000 cm^{-1} ($\tilde{o}_{as}$ Si-O-Si) and 770-420 cm^{-1} ($\tilde{o}_{s}$ Si-O-Si and Si-O_t) of the microcline spectra were also present in the residues. Bands around 3754 cm^{-1} in the Alfisol and Mollisol weathered residues and that around 2370 cm^{-1} in all three residues originate from the respective HAs. These confirm the precipitation of HAs on the surface of the mineral.

Conclusions

The alternate peak-trough nature of cation dissolution from silicates is indicative of successive dissolution – precipitation cycles in contrast to the steady increments observed with aqueous or acid dissolution. Dissolution of epidote follows the general order : $Fe^{2+/3+} > Al^{3+} > Ca^{2+} > Si^{4+}$ except with Mollisol HA where $Ca^{2+} > Al^{3+}$. Entisol and Alfisol HAs seem to be more effective dissolution agents than Mollisol HA. With microcline, Al^{3+} release far exceeded that of Si^{4+}. The general pattern of dissolution is incongruent. No significant effect of pH is observed.

The study of altered products of mineral-HA reaction shows a marked reduction in Si^{4+}, $Fe^{2+/3+}$, Ca^{2+} but enrichment of Al^{3+} with epidote residues and slight reduction in Si^{4+}, $Fe^{2+/3+}$, K^{+} and enrichment of Al^{3+} with microcline residues. The XRD bands of the weathered residues changed considerably with the formation of new crystalline phases containing Ca^{2+}. In contrast, the XRD bands of microcline was less affected and no new crystalline phase was detected. The IR spectral bands of both epidote and microcline were mostly retained in their weathered residues. However, there is an indication of HA precipitation on the mineral surface.

Acknowledgements

The funding received from Indian Council of Agricultural Research is being gratefully acknowledged. The authors are also grateful to Professor A Patra, Department of Chemistry, University of Calcutta, Kolkata for IR and Dr. DK Pal, Division of Soil Resource Studies, NBSS & LUP, Nagpur for XRD analyses.

References

Barman, A.K., Varadachari, C. and Ghosh, K. 1992. Weathering of silicate minerals by organic acids. I. Nature of cation solubilisation. *Geoderma* **53**: 45-63.

Bennett, P.C. 1991. Quartz dissolution in organic-rich aqueous systems. *Geochim. Cosmochim. Acta* **55**: 1781-1797.

Das, S., Ghosh, K. and Varadachari, C. 2013. Weathering of silicate minerals by humic acids : I. Nature of cation solubilisation from olivine and tourmaline and characteristics of the residual products. *Clay Res.* **32** : 58-75.

Das, S., Ghosh, K. and Varadachari, C. 2014. Weathering of silicate minerals by humic acids : II. Nature of cation

solubilisation from hornblende and biotite and characteristics of the residual products. *Clay Res.* **33** : 46-63.

Deer, W.A., Howie, R.A. and Zussman, J. 1985. *An Introduction to the Rock-forming Minerals*. ELBS-Longman, Harlow.

Drever, J.I. 1997. Weathering processes. In (O.M. Saether and P.de. Caritat, Ed.), *Geochemical Processes, Weathering and Groundwater Recharge in Catchments*. A.A. Balkema, Rotterdam, pp. 3-19.

Farmer, V.C. and Russel, J.D. 1964. The infrared spectra of layer silicates. *Spectrochim. Acta* **20**: 1149-1173.

Furrer, G. and Sticher, H. 1999. Böden als Naturkörper-Chemische Verwitterungsprozesse. In *Handbuch der Bodenkunde*, Landsberg/Lech, Germany, pp. 1-16.

Ghosh, K. and Schnitzer, M. 1979. UV and visible absorption spectroscopic investigations in relation to macromolecular characteristics of humic substances. *J. Soil Sci.* **30:** 735-745.

Golubev, S.V. and Pokrovsky, O.S. 2006. Experimental study of the effect of organic ligands on diopside dissolution kinetics. *Chem. Geol.* **235**: 377-389.

Hansley, P.L. and Briggs, P.H. 1994. Garnet dissolution in oxalic acid : A possible analog for natural etching of garnet by dissolved organic matter. *U. S. Geol. Survey Bull.* **2106**: 1-14.

Hees, P.A.W. van and Lundstrom, U.S. 2000. Equilibrium models of aluminium and iron complexation with different organic acids in soil solution. *Geoderma* **94**: 201-221.

JCPDS, 1967, 1972, 1979, 1980, 1983, 1984. *Powder Diffraction File*. Joint Committee on Powder Diffraction Standards, Pennsylvania, USA.

JCPDS, 1987. *Powder Diffraction File*. International Centre for Diffraction Data, Swarthmore, USA.

Knauss, K.G. and Copenhaven, S.A. 1995. The effect of malonate on the dissolution kinetics of albite, quartz and microcline as a function of pH at 70°C. *Applied Geochem.* **10**: 17-33.

Kononova, M.M. 1966. *Soil Organic Matter*. Pergamon, Oxford.

Schalscha, E.B., Appelt, H. and Schaltz, A. 1967. Chelation as a weathering mechanism. I. Effect of complexing agents on the solubilization, of iron from granodiorite. *Geochim. Cosmochim. Acta* **31**: 587-596.

Stumm, W. and Furrer, G. 1987. The dissolution of oxides and aluminium silicates; Examples of surface-co-ordination-controlled kinetics. In (W. Stumm, Ed.), *Aquatic Surface Chemistry– Chemical Processes at the Particle-water Interface*. Wiley- Interscience, New York, pp. 197-219.

Stumm, W. and Wieland, E. 1990. Dissolution of oxide and silicate minerals : Rates depend on surface speciation. In (W. Stumm, Ed.), *Aquatic Chemical Kinetics*. Wiley, New York. pp. 367- 400.

Varadachari, C., Barman, A. K. and Ghosh, K. 1994. Weathering of silicate minerals by organic acids. II. Nature of residual products. *Geoderma* **61**: 251-268.

Welch, S. A. and Ullman, W. J. 1996. Feldspar dissolution in acidic and organic solutions : Compositional and pH dependence of dissolution rate. *Geochim. Cosmochim. Acta* **60**: 2939-2948.

Wit, H.A., De, G.T. and Mulder, J. 2001. Predicting aluminium and organic matter solubility using the mechanistic equilibrium model WHAM. *Soil Sci. Soc. Am. J.* **65**: 1089-1100.

Wogelius, R. A. and Walther, J. V. 1992. Olivine dissolution kinetics at near-surface conditions. *Chem. Geol.* **97**: 101-112.

(Received February 2015; Accepted May 2015)

ACKNOWLEDGEMENT

CMSI acknowledges the revising/editing of the following persons:

1. Dr. D.K. Pal
2. T.K. Bhattacharyya
3. K.M. Manjaiah

INSTRUCTIONS FOR CONTRIBUTORS

CLAY RESEARCH is the official publication ofTHE CLAY MINERALS SOCIETY OF INDIA and is published twice a year, in June and December. The Journal undertakes to publish articles of interest to the international community of clay scientists, and will cover the subject areas of mineralogy, geology and geochemistry, crystallography, physical and colloid chemistry, physics, ceramics, civil and petroleum engineering and soil science.

The Journal is reviewed in *Chemical Abstracts, MineralogicalAbstracts, and Soils and Fertilizers.*

Paper (in English) should be submitted to the Editor, Clay Research **"The Clay Minerals Society of India"** Division of Soil Science and Agricultural Chemistry, I.A.R.I., New Delhi-I to 012. E-mail: samar_I953@yahoo.com. At least one of the authors should be member of THE CLAY MINERALS SOCIETY OF INDIA. Submission is an undertaking that the manuscript has not been published or submitted for publication elsewhere.

Manuscripts should not exceed sixteen typed (double spaced) pages including tables and illustrations. **The original and two copies oftext and illustrations should be submitted.**

Form Manusciprts should be typewritten, double spaced on white paper, with wide margins. Intending contributors should consult a recent issue of CLAY RESEARCH for the standard format and style. The manuscript should have the sections ABSTRACT, introductory portion (untitled), MATERIALS AND METHODS, RESULTS and DISCUSSION and REFERENCES.

Title page should contain manuscript title, full name(s) of author(s), address (es) of the institution(s) of the author(s), a short running title not exceeding 60 characters including spaces, footnotes if any to the title, and complete mailing address of the person to whom communications should be sent.

Abstract should be a condensation of the ideas and results of the paper. It should not exceed 25'0 words. Do not make reference to the literature in the abstract.

Tables should have the simplest possible column headings. Type each table on a separate page; indicate location in the text by marking in the margin of text page.

Figures should be self-illustrative, drawn with black India ink on tracing paper or white Board. The lattering should be large enough to permit size reduction to one Journal page column width (about 7.0 cm) without sacrificing legibility. **The original tracing should be submitted**. The size of the drawing should not exceed 24 × 17 cm. Give the numbered legend on a separate sheet, not on the figure itself. Data available in the tables should not be duplicated in the form of illustrations. Indicate the location of the figure in the text by marking in the margin of the page.

Photographs should be in the form of glossy prints with strong contrast. In photomicrographs, the scale in micron or other suitable unit should be drawn on the print. Give the numbered legend on a separate sheet. Indicate the location of the photograph in the text by making in the margin of the text page.

References should be cited in the text by the name(s) of author(s) if two or less, and year of publication. If there are more than two authors, give the name ofthe first author followed by *'et al'* and year. Full references giving author(s) and initial(s), year, title of paper, (journal, volume, number if paged separately), first and last pages should be listed alphabetically at the end of the paper. Journal title should be abbreviated in accordance with the World List of Scientific Periodicals and its sequences.
Examples are

Grim, R.E., Bray, R.H. and Bradley, W.R. 1937. The mica in argillaceous sediments. *Am. Miner.* **22**:813-829.

Brindley, G.W. 1961. Chlorite minerals. In *(G.* Brown, Ed.) *The X-ray Identification and Crystal Structures of Clay Minerals,* Mineralogical Society, London, pp.242-296.

Theng, B.K.G. 1974. *The Chemistry of Clay Organic Reactions,* Adam. Hilger, London, 343 pp.

Review Every manuscript submitted to CLAY RESEARCH is independently reviewed by one or more referees. Acceptance or rejection of a manuscript is the responsibility of the Editor.

Reprints No free reprints are supplied to authors. Order for priced reprints should be sent when required by the Editor.

Clay Research

Vol. 33 **December 2014** **No. 2**

CONTENTS

Printed at : Cambridge Printing Works, New Delhi-1100028. (Mobile : 9811860113)